THESIS

# SHAPE-MORPHING ROBOTIC FISH

Submitted by

Clint Middlemist

Department of Mechanical Engineering

In partial fulfillment of the requirements

For the Degree of Master of Science

Colorado State University

Fort Collins, Colorado

Spring 2025

Master's Committee:

Advisor: Jianguo Zhao

Mostafa Yourdkhani
Thomas Bradley

ABSTRACT

SHAPE-MORPHING ROBOTIC FISH

Robotic fish have gained attention for their potential applications in underwater exploration, environmental monitoring, and bio-inspired robotics research. These systems aim to replicate the efficient propulsion and maneuverability observed in biological fish. However, current robotic fish designs are limited by their fixed stiffness and inability to dynamically adapt to varying environmental conditions. Traditional solutions for modulating stiffness or morphology often rely on bulky hardware or complex external systems, limiting scalability and versatility.

This thesis addresses these limitations through the development of an embedded morphing scheme that integrates actuation, sensing, and shape-locking mechanisms directly into the robot's structure. Utilizing Shape Morphing Modules (SMMs) composed of Shape Memory Polymers (SMPs) and Twisted and Coiled Actuators (TCAs), this scheme enables compact and efficient systems capable of real-time stiffness and shape modulation. Beyond robotic fish, this scheme demonstrates versatility in applications such as adaptive grippers, reconfigurable surfaces, and robotic manipulators requiring dynamic morphing.

We first implemented the embedded morphing scheme in a robotic fish with a variable-stiffness tail. The tail's stiffness was adjusted by controlling the curvature of thin plates via TCAs, with the shape locked by SMP ribs. Experimental results revealed improved adaptability for both speed and maneuverability under different conditions, though excessive stiffness caused buckling under high forces, indicating a trade-off between stiffness and structural limits.

The embedded morphing scheme was extended to a robotic fish with a morphing body to explore the relationship between body shape and swimming performance. Modified SMMs allowed for dynamic changes in body depth and width. The fish was controlled using a Central Pattern Generator (CPG) model, which enabled precise tuning of swimming parameters such as frequency,

amplitude, and phase offset. Testing showed that body shape significantly influenced swimming performance, with a flat-flat configuration yielding higher speeds compared to a medium-large configuration due to reduced drag.

# ACKNOWLEDGEMENTS

First, I would like to thank my wife, friends, and family for their unwavering support through my journey to obtain my masters. I would not be where I am today without your love and encouragement. From the bottom of my heart, thank you. I would like to thank my research colleagues for their guidance and assistance during this process. Bryce Jones, Sydney Speigel, Eli Lerner, and the many others, I thank you for providing assistance and guidance when I needed it most. I also want to thank Dr. Mostafa Yourdkhani and Dr. Thomas Bradley for their time, guidance, and feedback as committee members for my work. Finally, I want to thank my advisor, Dr. Jianguo Zhao, for the past three and half years of guidance. His mentorship molded me to the engineer I am today.

# DEDICATION

*I would like to dedicate this thesis to my wife, Emily. Your love, support, and kindness on the days I needed it most were the fuel to push me to the finish line. I wouldn't be the man or engineer I am today without you. I love you.*

TABLE OF CONTENTS

LIST OF TABLES

LIST OF FIGURES

# Chapter 1

# Introduction

## 1.1 Background and Previous Work

The goal of this research is to advance the field of bio-inspired robotics by integrating novel shape-morphing capabilities into robotic fish. These capabilities aim to dynamically optimize swimming performance through tunable stiffness and adaptive morphing mechanisms, addressing critical gaps in current designs. To achieve this, the work leverages advancements in shape-morphing materials, such as shape memory polymers (SMPs) and twisted and coiled actuators (TCAs), to create an embedded shape morphing scheme capable of morphing in a variety of environments. The following sections provide an overview of the relevant background and previous research, including shape-morphing robotics, twisted and coiled actuators, tunable tail stiffness in robotic fish, the application of central pattern generators (CPGs), and the influence of body morphology on swimming performance.

### 1.1.1 Shape Morphing Robots

Biological organisms exhibit remarkable shape-morphing capabilities, enabling them to adapt their forms in response to environmental changes or evolutionary pressures. This adaptive morphology, observed across species—from the metamorphosis of caterpillars to butterflies to the shape-shifting limb structures of amphibious animals—provides diverse advantages for survival across different habitats. Inspired by nature's flexibility, shape-morphing capabilities are now a focal point in robotic and materials science, aiming to design systems that can switch functionalities based on environmental demands.

Within the field of soft robotics, shape memory polymers (SMPs) and other adaptive materials are central to achieving versatile, untethered morphing. For instance, SMPs can change stiffness upon heating, offering structural adaptability critical for load-bearing applications. SMP compos-

ites embedded with magnetic particles allow for even more complex, programmable deformations by combining shape retention with magnetic responsiveness, shown in Fig. 1.1E, where heating-induced softening paired with a magnetic field facilitated rapid, reversible transformations in the material [2]. This advancement enables multifunctional applications such as soft robotic grippers or morphing antennas that require high adaptability and strength.

Similarly, layer-jamming mechanisms as seen in Fig. 1.1F, as discussed by Kim et al. (2013), employ frictional forces between layers to achieve variable stiffness, supporting minimally invasive surgery devices that can transition between flexible and rigid states on demand. This tunable stiffness mechanism has broad applications in medical robotics and adaptable manipulators, as it enables both pliability for safe insertion and rigidity for stability once in place [3].

Another notable contribution is from adaptive morphogenesis, as demonstrated in a study on robotic turtles that transition between aquatic and terrestrial environments by Baines et al. (2022). This morphing limb structure, seen in Fig. 1.1A, integrating stimulus-responsive materials, allows the robotic limbs to transform from load-bearing to hydrodynamic forms depending on the environment, enhancing efficiency and maneuverability [1]. The robot is capable of walking, crawling, and swimming, as shown in Fig. 1.1B-D.

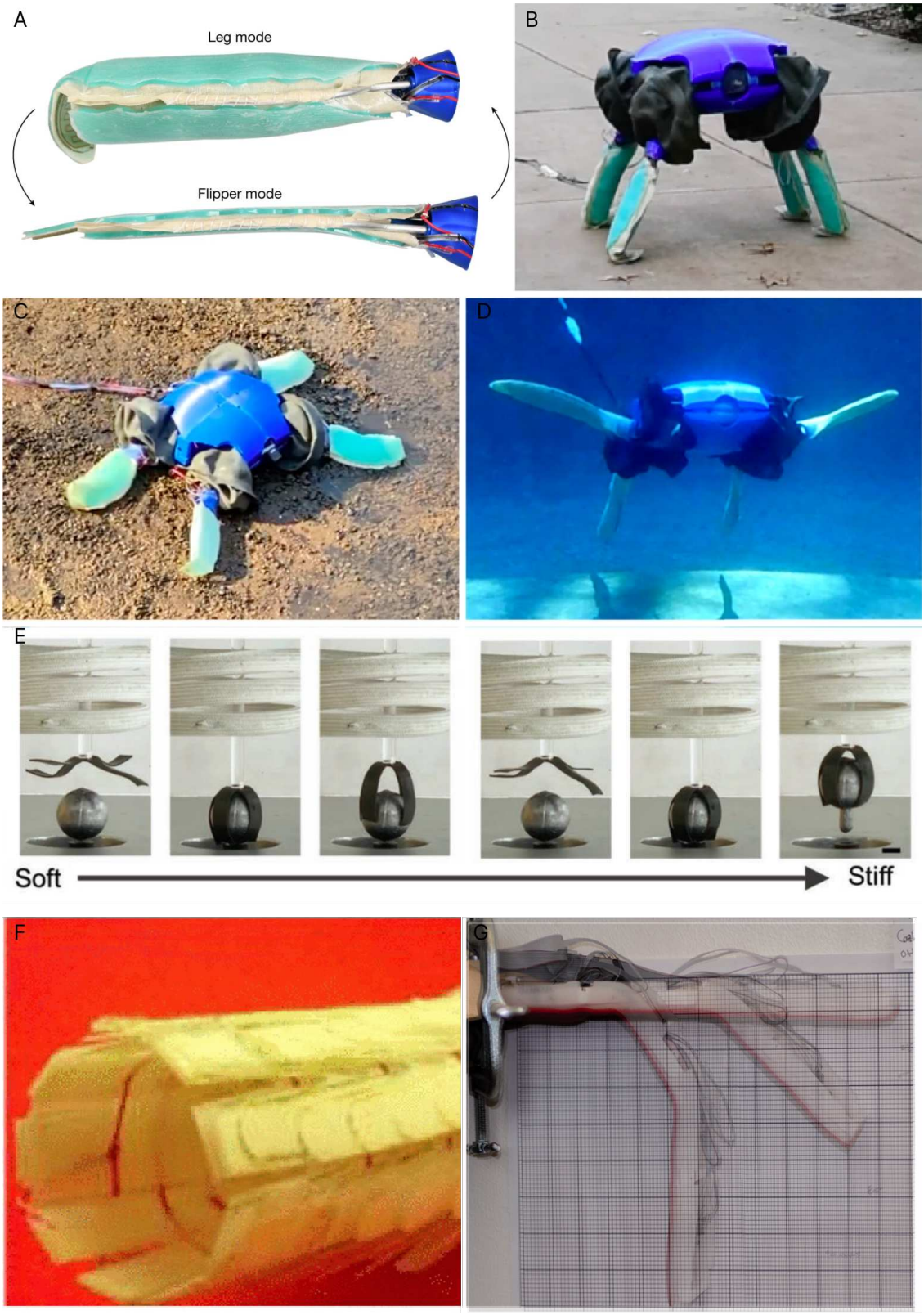


**Figure 1.1:** A) Side profile of morphing turtle leg [1]. B) Morphing turtle is capable of walking, C) crawling, and D) swimming [1]. E) Magnetic shape memory polymer is capable of varying stiffness to grasp objects [2]. F) Layer-jamming can be used to vary stiffness in surgical devices [3]. G) Thermoplastic composites with embedded actuators and sensor can localize stiffness variation [4].

Emerging advancements in thermoplastic composites further expand the scope of shape-morphing materials. McEvoy and Correll (2014) demonstrated that embedding sensors and actuators within thermoplastics enables localized stiffness variation controlled by heat, seen in Fig. 1.1G. This capability permits structural adjustments without additional components, promising innovations in adaptive casts, seating, and aerodynamic surfaces [4]. Similarly, the research by Davidson et al. (2019) on dielectric liquid crystal elastomers provides a pathway for actuators with fast response rates, integrating efficiency with programmable shape transformations that could benefit various soft robotic applications [11]. Other researchers have used shape shifting lattices to accomplish similar morphing capabilities [12].

### 1.1.2 Twisted and Coiled Actuators

Twisted and Coiled Actuators (TCAs) were first introduced by Haines et al. in 2014, marking a significant advancement in artificial muscle technology due to their inexpensive materials, high cycle life, and high energy density [5]. TCAs are created by twisting polymer fibers to a point where they create a larger coil. Depending on the direction of twist relative of the larger coils (chirality), the actuator responds to thermal activation with either contraction and expansion, as shown in Fig. 1.2. The functioning principle of a TCA arises from thermal activation (normally Joule heating), which causes the polymer fibers to untwist slightly, inducing torsion along the length of the actuator. This torsional force then creates an axial force within the larger coils, resulting in the contraction/expansion as the temperature changes. However, one downside of this design is the need to pre-load the TCA to separate the larger coils in order for it to function. This design constraint severely limits the applications of the actuator. However, one notable variation is the free-stroke TCA, which can contract up to 48% of its natural length without the need for a pre-load [13]. The fabrication processes of free-stroke TCAs includes similar steps to a normal TCA, but with an added step of wrapping the twisted thread around a helical mandrel with a prescribed distance between coils, as shown in Fig. 1.1.2. This versatility has led to numerous variations of TCAs, each tailored to specific robotic applications [13].

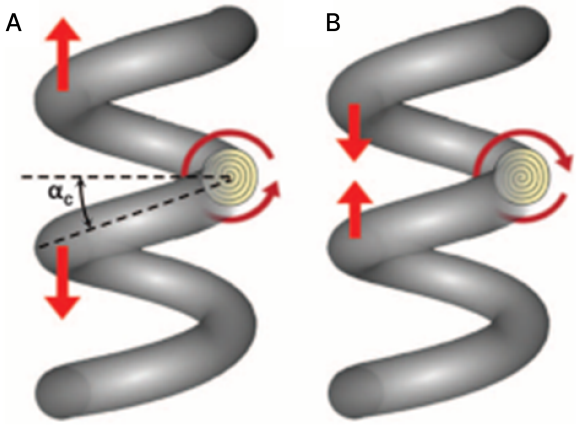


**Figure 1.2:** (A,B) Schematic representation of torsional fiber actuation mechanisms driving large-stroke tensile actuation of TCAs: (D) heterochiral coiled fibers that expand during heating and (E) homochiral coiled fibers contract during heating [5].

**Self-Sensing in TCAs** Self-sensing is a critical capability for TCAs, particularly in real-time control applications. In essence, self-sensing refers to the use of an actuator's existing properties—such as electrical resistance—to infer real-time operational parameters like force or displacement, without requiring additional sensors. A variety of methods have been used for self-sensing, including electrical impedance [14], temperature [15–17], and electrical resistance [18]. However one of the main drawbacks of most self-sensing methods is the need for additional materials (ex. nickel wire wrapped around TCA) or large and complicated equipment.Monitoring the electrical resistance of the actuator as it changes with temperature and deformation, however, does not require any expensive equipment or additional materials [19]. This approach leverages the inherent material properties of conductive fibers to create a feedback loop that provides control over actuation with minimal added complexity. The model developed by Wu et al. [18], and used by Sun, et al. [19] is defined as:

$$R = g(T(x, F), x, F) = h(x, F)$$

where $R$ is the electrical resistance of the actuator, $T$ is the temperature of the actuator, $x$ is the displacement of the actuator, and $F$ is the force exerted by the actuator.

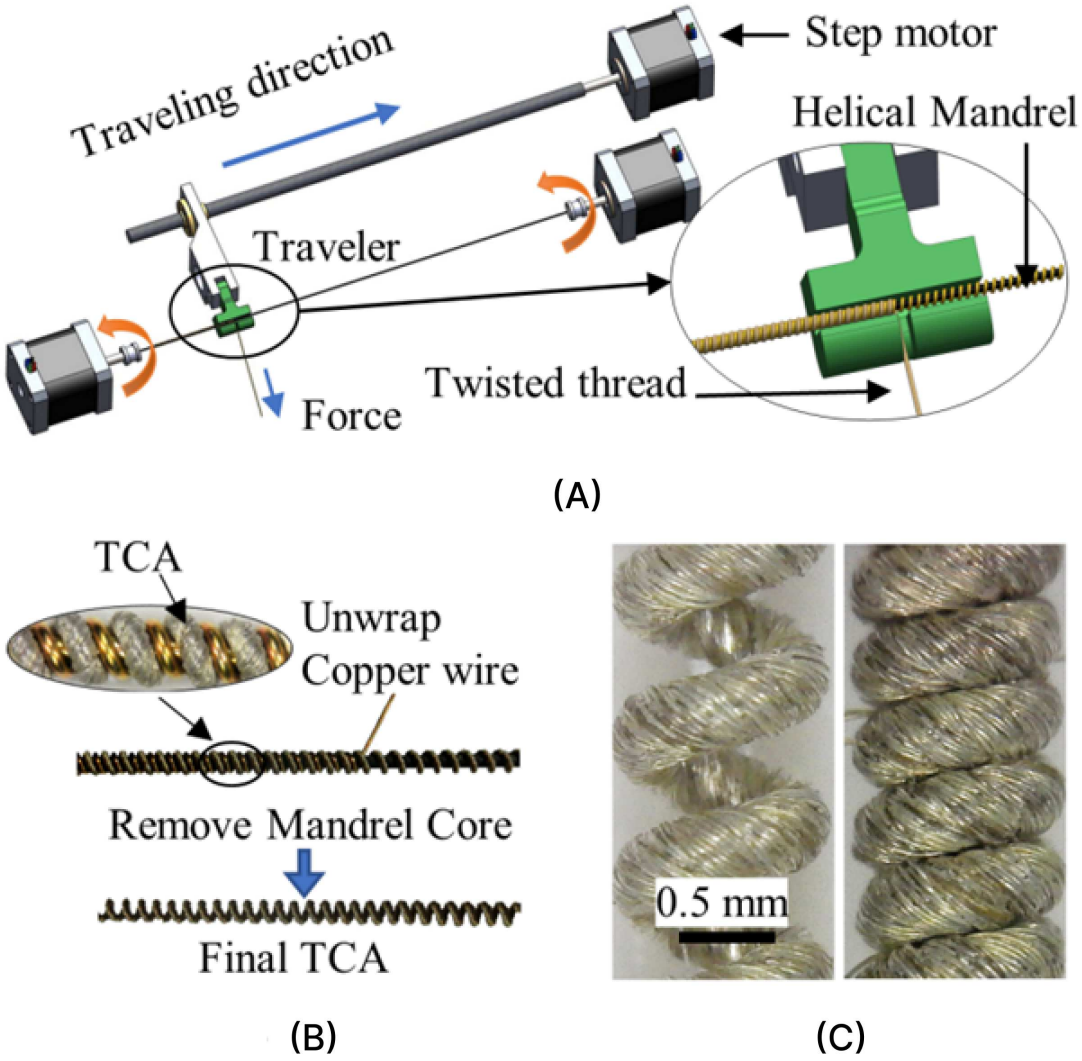


**Figure 1.3:** Fabrication process of the TCA: (A) Twisted fiber coiled onto a helical mandrel. (B) TCA removed from the mandrel following annealing. (C) Microscopic images of the TCA at room temperature (left) and after heating (right) [19].

### 1.1.3 Robotic Fish with Tunable Tail Stiffness

Robotic fish are widely researched for their potential to replicate the efficient propulsion and maneuverability of biological fish. In nature, fish demonstrate a range of swimming capabilities, from high-speed cruising to precise maneuvering, by adjusting the stiffness of their fins and body musculature to suit their environment. This dynamic adaptation is challenging to replicate

in robotic systems, where fixed stiffness limits flexibility and makes it difficult to optimize for both speed and maneuverability. The development of tunable stiffness mechanisms in robotic fish addresses these limitations by enabling real-time adaptation of tail stiffness, thereby improving performance in varying conditions. The trade-off between speed and maneuverability is a core

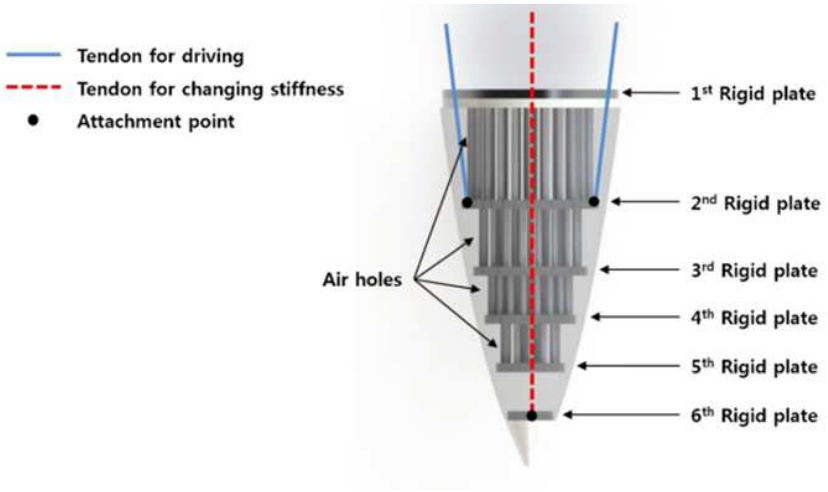


**Figure 1.4:** Design of the driving component of a robotic fish with a variable-stiffness structure and tendons: red dashed line indicates the tendon for stiffness adjustment, blue solid lines represent driving tendons, and dots mark attachment points [6].

design consideration in robotic fish. Generally, a stiffer tail structure allows for faster, more powerful swimming at higher tail frequencies, which is ideal for straight-line propulsion and energy efficiency over long distances. Conversely, a more flexible tail increases maneuverability, allowing the fish to make tighter turns and navigate complex environments. This balance between speed and maneuverability is particularly relevant for robotic applications in underwater exploration, where rapid directional changes are sometimes as important as sustained forward motion. By modulating tail stiffness, robotic fish can achieve a balance between these performance metrics, adapting to different operational demands [20–25] [26]. Several researchers have explored innovative ways to incorporate variable stiffness mechanisms into robotic fish tails, each contributing to the field's understanding of stiffness modulation and its effects on swimming performance. Park et al. developed a variable stiffness flapper, an innovative design that adjusts stiffness to maximize thrust under

different swimming frequencies. The device, shown in Fig. 1.4, incorporates an endoskeleton with alternating compliant and rigid segments [6]. By adjusting the tension on embedded tendons, the flapper's stiffness can be modulated to optimize performance across a range of speeds. When the tendons are tightened, the flapper becomes stiffer, enabling higher thrust at higher frequencies. At lower tensions, the flapper gains flexibility, enhancing maneuverability. This approach demonstrates how stiffness modulation can be used to achieve a versatile swimming performance that adapts to different environmental conditions. Another approach to tunable stiffness in robotic fish

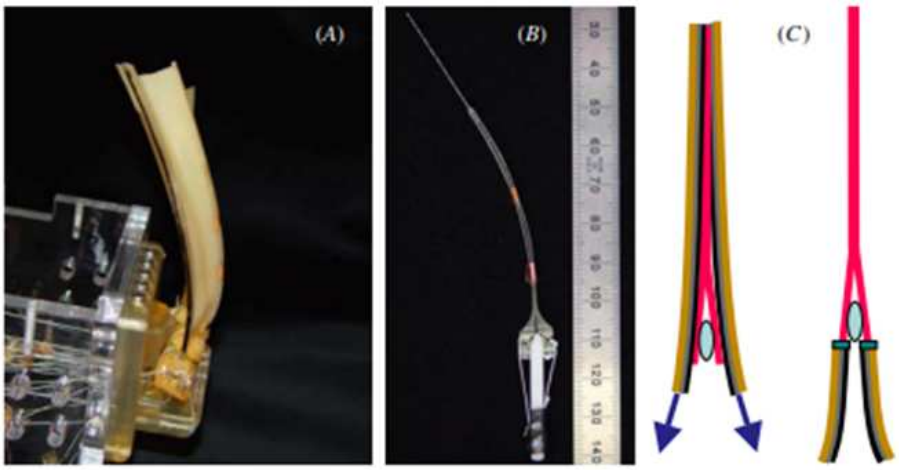


**Figure 1.5:** The shape and stiffness of a robotic fin (A) are adjustable by controlling the curvature of individual fin rays (B). This is achieved by displacing the base of one half of the fin ray relative to the other half, where a 1 mm base displacement results in a 30 mm tip displacement. (C) CAD rendering illustrates potential integration of linear actuators along the fin ray bones or attached at their bases [7].

is the use of ionic polymer-metal composite (IPMC) actuators, as demonstrated by Tangorra et al.. IPMC actuators are soft, flexible materials that can change shape when an electric field is applied, effectively altering stiffness and providing propulsion. Tangorra's fins, depicted in Fig. 1.5, exhibit lifelike undulatory motion that can be controlled to vary both the stiffness and the frequency of fin movements [7].

### 1.1.4 Central Pattern Generation in Robots

Central Pattern Generators (CPGs) are neural circuits that produce rhythmic outputs without requiring sensory input or higher neural control. These circuits play a key role in biological locomotion and have been adapted for use in robotics to generate rhythmic motion in systems like robotic fish or snake-like robots. At their core, CPGs rely on mathematical models to simulate rhythmic oscillations.

The Matsuoka oscillator is one widely used mathematical framework for CPGs [27]. It represents a continuous-variable system that models the dynamics of mutual inhibition and adaptation between neurons. In a simple configuration, a CPG module consists of two mutually inhibiting neurons. This dual-neuron model generates rhythmic outputs through alternating activation. The output signal is defined as the difference between the two neurons' outputs: $y_{out} = y_1 - y_2$ [8]. Each module in a network has their own dual-neuron system, and the inter-connectivity between the modules can be adjusted depending on the system [8]. This can be seen in Fig. 1.6, where the modules are connected in a unilateral network to provide coherent, oscillatory motion.

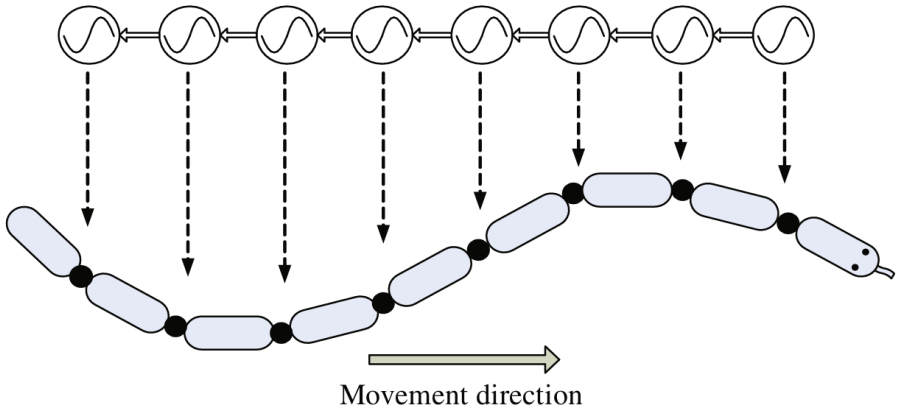


**Figure 1.6:** CPG network implemented into a snake-like robot. Each module has their own dual-neuron system, which is interconnected [8].

This mutual inhibition prevents the system from settling into a stable state, resulting in continuous oscillations. The periodic signal can be directly applied to control the motion of robotic joints or segments, making the system ideal for rhythmic tasks like undulatory swimming or crawling.

By adjusting parameters such as time constants, adaptation coefficients, and coupling weights, the CPG's output can be tuned to achieve desired motion characteristics like frequency and amplitude. This flexibility, combined with the simplicity of the dual-neuron model, has made CPGs a powerful tool for achieving bio-inspired locomotion in robotics.

### 1.1.5 Body Morphology and its Impact on Swimming Performance of Biological and Robotic Fish

The overall shape and characteristics of a fish's body play critical roles in determining swimming speed, efficiency, and maneuverability. Body length, depth, and shape all play an impact into swimming performance [28]. Webb et al. in 1984 proposed that some fish are specialized for cruising, accelerating, or maneuvering, which lies on a functional-morphology plane to categorize fish [28]. Similarly, Bandyopadhyay et al. categorized 28 species of fish by speed and maneuverability [29]. Along with this, body shape plays a key role in the stability during swimming and maneuvering [30]. While studying two different species of tetra with different body depths,

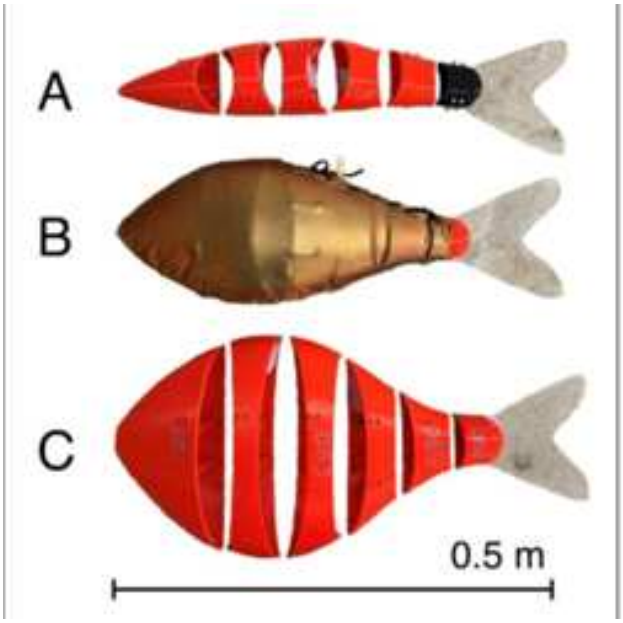


**Figure 1.7:** Body shells for a robotic fish varying in body depth: (A) shallow, (B) medium,(C) deep. The medium shape shows the fully assembled robot with tailored skin [9].

(*Gymnocorymbus ternetzi and Aphyocharax anisitsi*), differences in turning performance were observed and analyzed [9]. To isolate the effects of body depth, Howe et. al. found that increasing body depth in robotic fish increased centripetal acceleration, a key factor in maneuverability [9]. Through another biological study, Cai et al. found that burst speed, induced flow velocity, and critical swimming speed all increase with body length [31]. Many others have developed robotic fish to closely mimic biological fish, with a focus on better understanding of natural species [32–35].

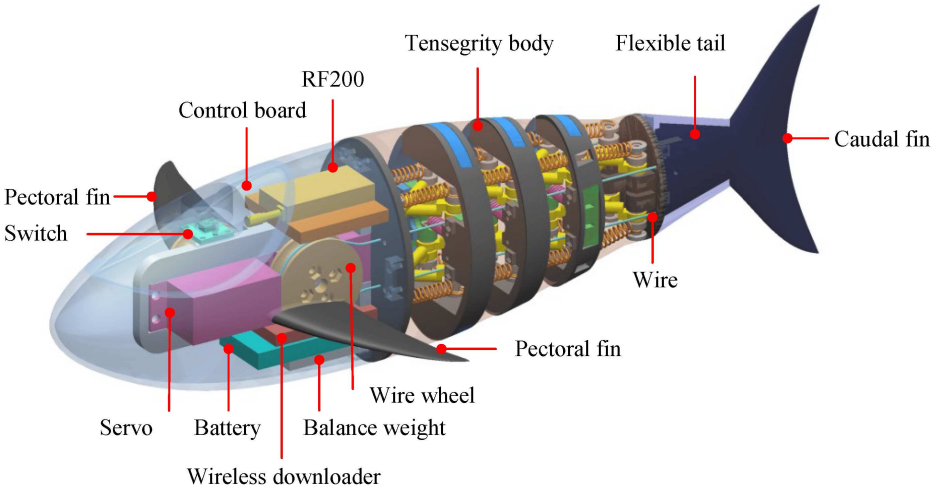


**Figure 1.8:** Mechanical design of a variable stiffness robotic fish that utilizes tensegrity structures within the body to modulate stiffness [10].

In addition to body dimensions, stiffness is another key factor influencing swimming performance. The stiffness of the body, similar to a tail, can have large impacts on swimming performance. This is noted by Long et al., in which biological fish utilize muscles on their body to adjust stiffness to generate negative work during swimming [36] . Researchers have both studies biological fish and developed robotic fish with tunable body stiffness mechanisms to address this trade-off, allowing for adjustments based on the desired swimming performance [10, 36–39]. One example, shown in Fig 1.8 utilizes a tensegrity mechanism to adjust the stiffness of the body.

Other researchers have attempted to manipulate speed and maneuverability through means of morphing other parts of the body as well. Huang et al., developed a tuna-like robotic fish capable

of morphing its dorsal fin to impact swimming [40]. Although the dorsal fin did not play much impact on swimming speed, it however improved the yaw stability of the robotic fish.

### 1.1.6 Gap in Current Research

The field of shape-morphing robotics has made significant strides in replicating biological adaptability through materials like SMPs, TCAs, and tunable stiffness mechanisms. These advancements have demonstrated the potential of variable stiffness and morphing capabilities to enhance robotic functionality across diverse applications, from underwater exploration to dynamic terrestrial locomotion. Furthermore, CPG-based control systems have shown great promise for generating rhythmic, lifelike movements, particularly in snake-like and fish-inspired robots.

However, most existing shape-morphing schemes rely on bulky external hardware or large power sources, limiting scalability and practicality in dynamic environments where compact, efficient, and untethered designs are critical. While materials like SMPs and TCAs have introduced the potential for lightweight and adaptive systems, similar systems often require extensive support systems. This reliance on external hardware leaves a significant gap in realizing fully integrated, self-contained morphing robots capable of dynamic and autonomous operation.

In the domain of robotic fish, significant progress has been made in developing tunable stiffness mechanisms, particularly for tail structures. However, these efforts predominantly rely on tendon-driven systems or variable material properties, with few, if any, designs incorporating true shape-morphing technologies for tail stiffness modulation. This gap represents a missed opportunity to dynamically adapt stiffness in real-time to optimize swimming performance for both speed and maneuverability.

Furthermore, the concept of body-wide morphing in robotic fish remains largely unexplored. While some studies have investigated how body stiffness and shape affect swimming dynamics, no existing designs implement active shape morphing along the entire body. This limitation constrains the ability of robotic fish to mimic the adaptability and efficiency observed in biological organisms. The integration of dynamic shape morphing along both the body and tail, combined with CPG-

based control systems, would enable robotic fish to achieve holistic performance optimization across varying swimming conditions.

Finally, while research has examined trade-offs between stiffness, swimming speed, and maneuverability, there has been limited exploration into how body shape and morphing parameters interact with control models like CPGs. This lack of understanding leaves a critical gap in the ability to fine-tune these parameters dynamically, further constraining the design of truly adaptive, bio-inspired robotic systems.

## 1.2 Contributions

- **Novel Embedded Shape Morphing Modules:** We present an embedded morphing scheme that integrates actuation, sensing, and locking mechanisms directly into a robot's body. To demonstrate the versatility of this technology, we present the working principle, design, and fabrication of the Shape Morphing Module (SMM). We then showcase the functionality of integrated sensing and actuation using TCAs within the SMM. These principles are then applied to a library of robots capable of grasping, and having a large variety of programmable shapes (torsion, 3D bending, and surface morphing). This embedded morphing scheme provides a robust solution for a variety of robotic applications in dynamic environments.

- **Robotic Fish with Shape Morphing Tail:** We utilize a modified version of the SMM to then create a variable-stiffness shape morphing fish tail, capable of adapting to various environments. Tail stiffness plays a critical role in swimming performance, with adjustments enabling a broad range of speeds and maneuverability. We showcase the stiffness changing mechanism, which utilizes SMMs to curve thin plates that comprise the tail to increase stiffness. This mechanism is then used to determine its impact on swimming performance by both turning and swimming speed.

- **Robotic Fish with Shape Morphing Body:** We again modify the original design of the SMM to create a robotic fish that utilizes shape morphing along the length of its body. Uti-

lizing three servo motors to control the motion of the fish, a model is developed using Central Pattern Generation to create a robust swimming gait. We then showcase the interconnection between body shape and varying swimming parameters (amplitude, frequency, phase offsets) in relation to swimming speed.

# Chapter 2

# Fabrication and Design of Shape-Morphing Modules

## 2.1 Introduction

Shape memory materials offer unique capabilities for systems requiring dynamic reconfiguration, yet many existing morphing strategies rely on external equipment or limited deformation modes. This section presents an embedded morphing scheme that integrates both shape actuation and deformation control within the material itself. The scheme enables versatile morphing behaviors, including twisting, bending, and hybrid forms, by using Shape Memory Polymer (SMP) spines or surfaces coupled with Twisted Coil Actuators (TCAs). By embedding this capability directly into the structure, the approach allows for precise and varied shape transformations without the need for external support. This framework is demonstrated through a library of morphing modules, each designed to showcase different deformation strains and topologies.

## 2.2 Working Principle and Fabrication of Shape-Morphing Module

The shape-morphing module (SMM) integrates actuation, sensing, and shape-locking capabilities within a single unit, leveraging a combination of shape memory polymers (SMP) and Twisted-and-Coiled Actuators (TCAs). Each component is carefully fabricated and designed to function in harmony, enabling dynamic shape changes in response to external inputs or environmental conditions.

**Working Principle.** The working principle of the embedded shape-morphing scheme is illustrated using a 2D bending module (115 mm × 6.5 mm × 5 mm) capable of achieving and maintaining various bending angles. This module employs a customized shape memory polymer (SMP) spine as its core, which enables the locking mechanism. SMP is selected for its unique proper-

ties: its elastic stiffness significantly decreases when heated above its glass transition temperature ($T_g = 100C$), allowing it to become pliable, and it can return to its original shape upon reheating due to its shape memory effect. The temperature of the SMP spine is controlled through Joule heating by embedding a resistance heating wire wrapped around the spine and a thermistor to monitor temperature, as seen in Fig. 2.1A.

Both actuation and sensing are accomplished by a twisted-and-coiled actuator (TCA), a thermally driven artificial muscle that contracts when heated and relaxes upon cooling. TCAs are ideal for this application because they operate at low voltages while providing a high energy density exceeding that of human muscles. Additionally, they can function as both actuators and self-sensing devices, eliminating the need for additional sensors that would be challenging to integrate due to heat generation, seen in Fig. 2.1B. The TCA is enclosed within a soft silicone tube, bent into a U-shape, and attached to the protrusions of the SMP spine, which can be sen in Fig. 2.1A. These protrusions are critical for minimizing thermal interference between the TCA and the SMP spine since both are thermally activated.

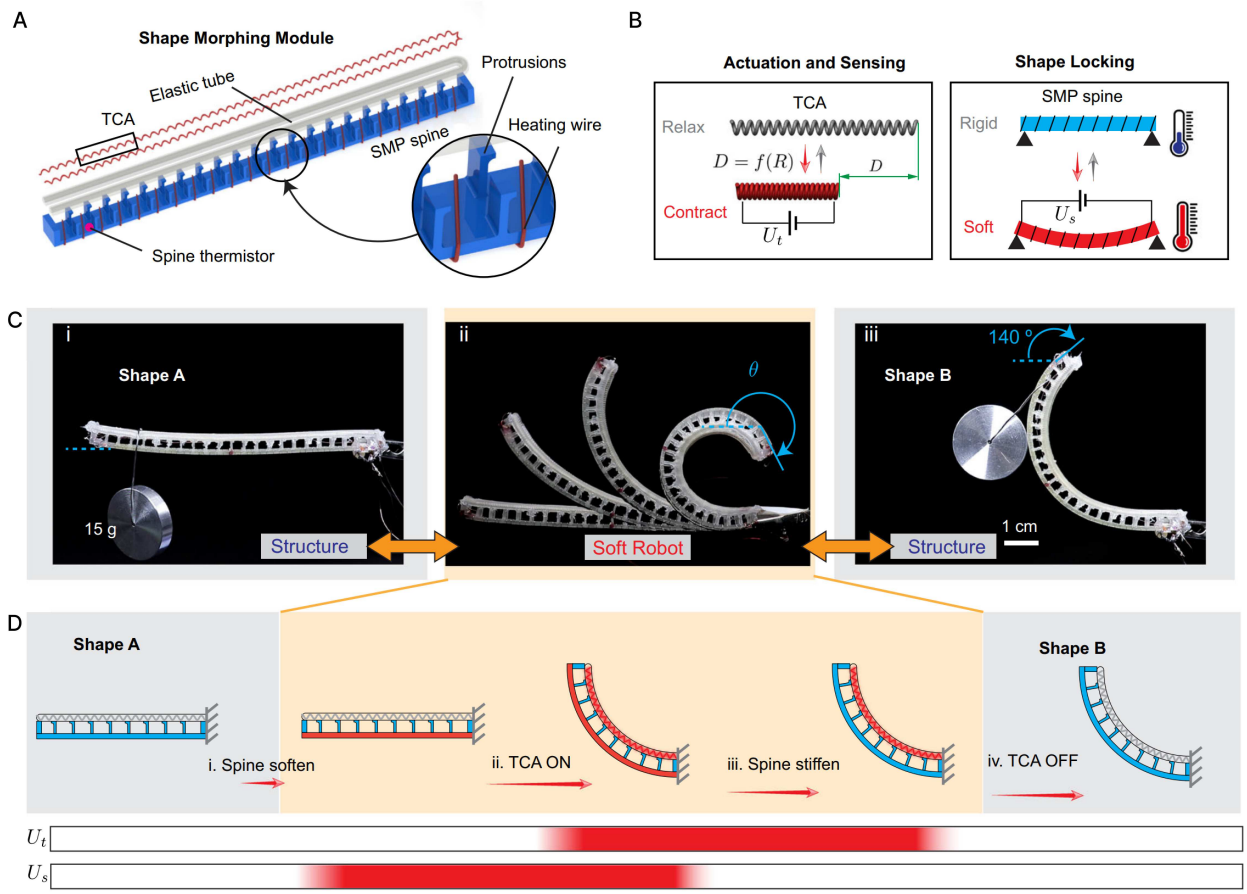


**Figure 2.1:** Shape Morphing Module (SMM) working principle. A) The 2D bending SMM consists of an SMP spine encased with heating wires, an elastic sheath, and a Twisted-and-Coiled Actuator (TCA) (center). B) Both actuation and sensing are achieved via the TCA, which contracts when an electrical current ($U_t$) is applied and relaxes as it cools. The TCA's resistance $R$ changes with displacement $D$. Shape locking is facilitated by the SMP spine, whose rigidity is modulated through Joule heating applied to the heating wire ($U_s$). C) Images showing the module during the morphing process. It can maintain a rigid shape to support a weight (left). When the spine is softened, the module behaves like a soft robot, allowing movement to different configurations (middle). After regaining stiffness, the module can hold a new shape securely (right). D) Sequence of the shape-morphing process: The module starts at shape A and transitions to shape B through the following steps: i) Heating wire ($U_s$) is activated, raising the spine's temperature above its glass transition temperature $T_g$ to soften it; ii) With the spine fully softened, the TCA is energized ($U_t$), causing it to contract and reshape the module; iii) Once the target shape is reached, the TCA maintains the configuration while the heating is turned off, allowing the spine to cool; iv) After the spine's temperature drops below 80°C and stiffness returns, the electrical input to the TCA ($U_t$) is removed, fixing the module in shape B, now ready to serve a different function.

The morphing process begins with the module in its initial straight shape ("Shape A") shown in Fig. 2.1C(i), functioning as a rigid structure capable of supporting a 15 g mass near its free end. To

initiate morphing, the spine is softened by applying a voltage ($U_s = 25V$ to the embedded heating wire. With the spine softened, the module transitions into a flexible state, shown in Fig. 2.1C(ii), allowing it to bend freely under the actuation of the TCA. For example, applying a constant voltage ($U_t = 3V$) to the TCA can bend the module to an angle of approximately 140°. Once the desired shape is achieved, the voltage applied to the heating wire is removed, allowing the spine to cool and regain rigidity. The TCA voltage is then turned off, locking the module into a new shape ("Shape B"), seen in Fig. 2.1C(iii), which can again support a 15 g mass without additional energy input. The module can return to its original straight configuration by reheating the SMP spine, utilizing its shape memory effect.

This morphing scheme is realized using compact, off-the-shelf electronic components in a self-contained setup, enabling efficient and versatile operation.

**Fabrication of the Shape-Morphing Module.** The fabrication process for the shape-morphing module starts with the construction of the SMP spine, which serves as the core structural component of the module. The spine is initially created through a 3D printing process and then used as a mold template for casting the SMP material. This SMP is chosen for its ability to exhibit significant stiffness variation when its temperature is raised above its glass transition point (approximately 100°C), allowing the material to shift between soft and rigid states. Depending on the application, the type of cure agent can be modified to change the properties of the SMP. For example, changing the cure agent from 3-Diethylaminopropylamine (6 percent by weight) to Jeffamine D-230 (38 percent by weight) will reduce the glass transition temperature of the polymer by approximately 20°C, making the polymer more suitable for different applications. Once the spine is cast, it is uniformly wrapped with a resistance wire (Nichrome 80- 38 AWG) to enable Joule heating, which controls the spine's temperature. For a majority of experiments, the temperature of the SMP spine is controlled via open loop control

The TCA is fabricated from conductive sewing thread, which undergoes a twisting, coiling, and annealing process to create its muscle-like properties. In our case, a machine was created to precisely fabricate TCAs, which helped to maintain consistency from actuator to actuator. To

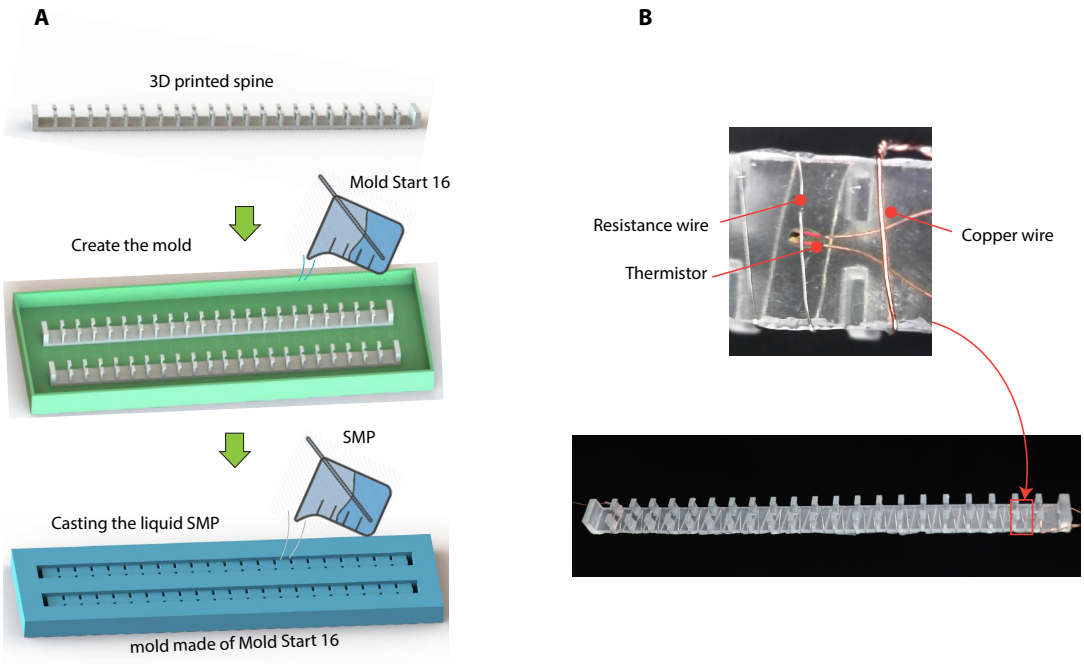


**Figure 2.2:** Fabrication of the SMP Spine for the 2D Bending Shape-Morphing Module (SMM). (A) The spine is first shaped using a Prusa SLA SL1S 3D printer. To create the mold, Mold Star 16 (Smooth-On Inc.) is poured into a container with the printed spine positioned at the bottom. The SMP liquid mixture is then poured into the mold and degassed using a vacuum oven. A flat, clear cover made from SORTA-Clear (Smooth-On Inc.) is placed on top to seal the mold. The SMP is cured at 75°C for 12 hours. (B) After curing, the SMP spine is wrapped with Nichrome resistance wire (AWG 38). A close-up view shows the embedded thermistor used for temperature monitoring.

start, a mandrel (copper wire, solid core, 26 AWG) is placed in the machine. Next, a guide wire (copper wire, solid core, 32 AWG) is wrapped around the mandrel by a series of stepper motors with specific revolution speed of the mandrel and linear velocity of the guide wire being wrapped around. Finally, the conductive sewing thread is twisted to nearly the point of coiling upon itself, and then coiled around the mandrel, following the guide wire. Once annealed, the guide wire and mandrel can be removed to reveal the TCA. Once removed, the TCA must be "trained" in order to repeatably actuate. To do this, the TCA is terminated at both ends using copper wire. One end is fixed to a vertical stand, and a 20g weight is hung from the other end. Power is then applied to the TCA (6.2V, 0.8A) and the TCA is contracted till the coils touch. This process is then repeated 5-10 times, in which the TCA is able to be used. This process is shown in Fig. 1.1.2. Once trained, the TCA is encased in a soft, elastic silicone sheath, providing protection against environmental

factors while maintaining flexibility. The sheathed TCA is then attached to the SMP spine by gluing the silicone sheath to the protrusions of the spine, combining the actuation element with the shape-locking mechanism.

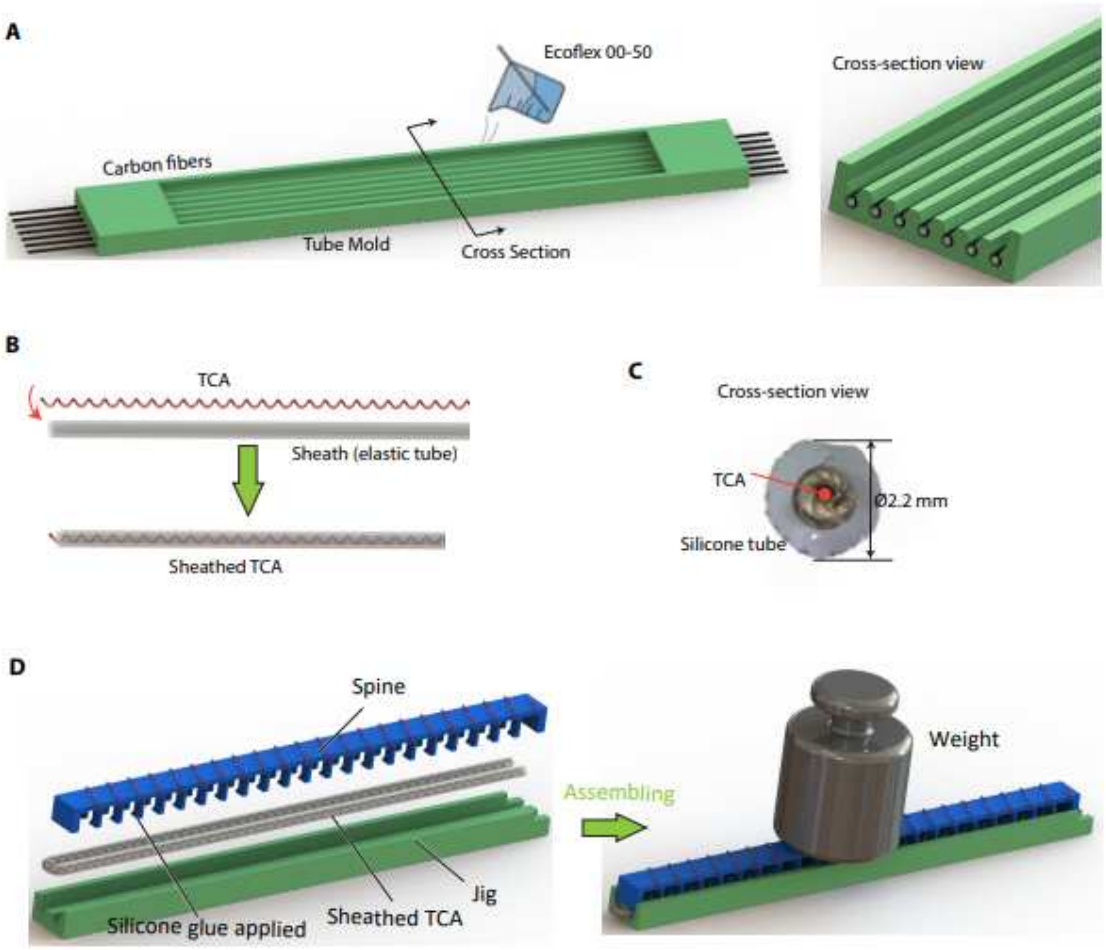


**Figure 2.3:** Fabrication of the Sheathed TCA and Assembly with the SMP Spine (A) The elastic tubes used as sheaths are fabricated using a 3D-printed mold, which can produce up to seven tubes simultaneously. The right image shows a cross-sectional view of the mold. (B) The sheathed TCA is created by inserting the Twisted-and-Coiled Actuator (TCA) into the fabricated elastic tube. (C) A cross-sectional view of the completed sheathed TCA reveals an outer diameter of 2.2 mm. (D) For the assembly of the sheathed TCA with the SMP spine, a jig is used to hold the TCA in a U-shaped configuration while securing the spine in position (left). During the curing process, a weight is placed on top of the spine to ensure proper bonding (right).

## 2.3 Closed-loop Control of the SMM using self-sensing of TCAs

Self-sensing actuators, like Twisted-and-Coiled Actuators (TCAs), provide a unique advantage by functioning simultaneously as actuators and sensors. This dual functionality simplifies the control architecture and reduces the complexity of robotic systems by eliminating the need for complex external sensors that could increase the weight or size of a robot. Specifically, self-sensing in TCAs occurs due to the correlation between electrical resistance and mechanical displacement during actuation. The ability to measure the TCA's resistance allows for real-time control of both force and displacement separately, making TCAs an excellent choice for applications requiring precise closed-loop control.

**Principle of Self-Sensing in TCAs.** Self-sensing in TCAs is achieved through their change in electrical resistance during actuation. The relationship between resistance $R$, temperature $T$, displacement $x$, and force $F$ is shown in Equation 1:

$$R = g(T(x, F), x, F) = h(x, F)$$

In this relationship, changes in temperature and displacement directly affect the resistance of the TCA, especially when the force is held constant during actuation. By maintaining a constant force, the resistance can be used as a reliable indicator of displacement. This direct correlation allows the electrical resistance of the TCA to be controlled in order to modulate its displacement.

**Control Circuit for Self-Sensing.** The control circuit used to monitor and adjust the resistance of the TCA is shown in 2.4. The system is designed to measure and control the resistance through voltage manipulation supplied to the TCA during actuation. A digital-to-analog converter (MCP4725) provides a reference voltage to a DC-DC buck converter (LM2596), which regulates the voltage supplied to the TCA. Additionally, a high-side current sensor (INA219) is used to monitor the current passing through the TCA, allowing for the real-time calculation of resistance using Ohm's Law:

$$R = V/I$$

Where $V$ is the voltage across the TCA and $I$ is the current through the TCA. By knowing both the voltage and the current, the system continuously calculates the resistance and adjusts the voltage to achieve the desired displacement.

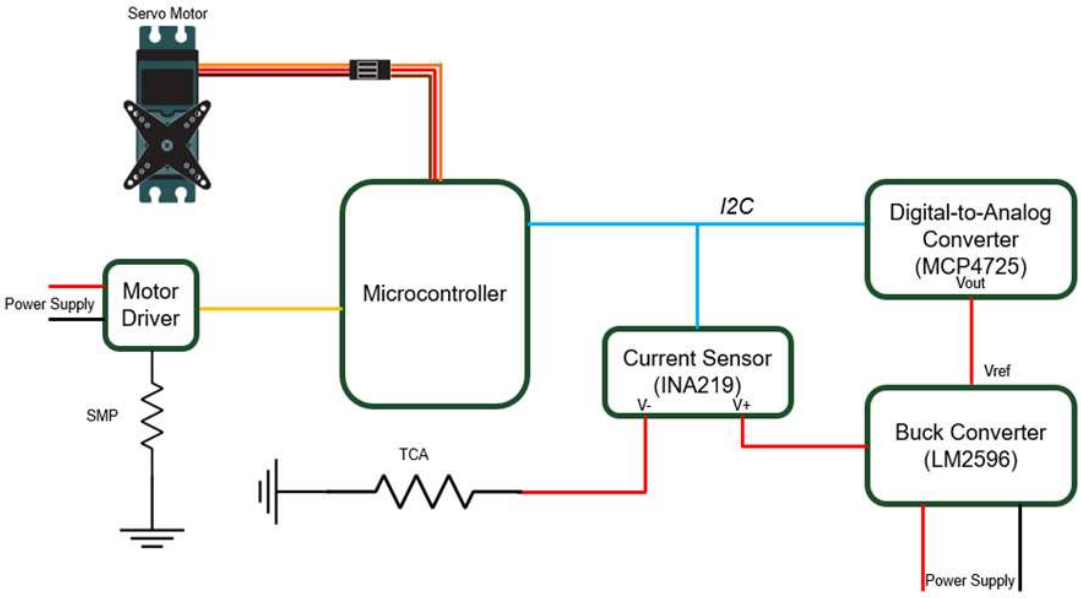


**Figure 2.4:** Circuit used to for self-sensing of TCA's combined with shape morphing. A microcontroller (Arduino Uno) is connected via I2C to both a current sensor (INA219) and Digital-to-Analog Converter (DAC) (MCP4725). As current flows from the power supply through the Buck Converter (LM2596) and through the TCA, the current sensor detects changes in current via a change in resistance. This change in resistance is used in closed loop control to provide a reference voltage from the DAC to the buck converter, controlling the TCA to the proper displacement.

**Closed-Loop Control of TCA** To control the TCA, the characterization of the resistance/ displacement relationship must first be established. This was accomplished through the use of the self-sensing circuit, shown in Fig. 2.4 to track resistance of the TCA during actuation, as well as directly measure displacement using a laser distance sensor placed directly underneath the TCA during actuation to capture real-time data of the TCAs displacement during actuation. The experimental setup can be seen in Fig. For the experiments conducted, the force was held constant

using a range of weights between 10g and 50 g, and the actuation velocity was regulated by applying a constant voltage of 10 V. The resistance-displacement relationship was then plotted for each weight, and a curve was fit to the relationship.

To ensure precise control of the TCA's displacement, a proportional-integral (PI) controller was implemented. The PI controller adjusts the rise time, overshoot, and steady-state error of the TCA's displacement by regulating the voltage applied to the TCA, depending on the change of resistance during actuation.

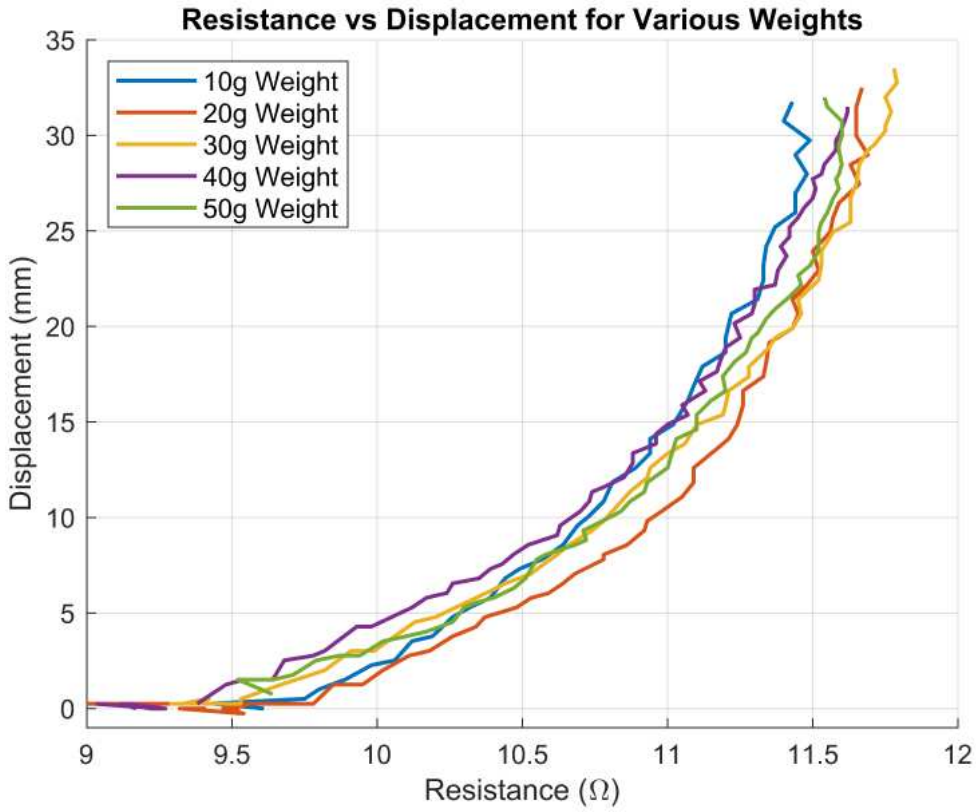


**Figure 2.5:** Resistance vs Displacement. For displacement experiments, a variety of weights from 10 g to 50 g were lifted to develop a characteristic equation.

Fig. 2.6 illustrates an experiment where the TCA was tasked with lifting a 20 g weight to a set-point displacement of 20 mm. Although achieving perfect control was not the primary goal, the PID controller was able to mitigate overshoot while minimizing oscillations during settling time.

However, the parameters could be further tuned to significantly reduce settling time and steady state error.

By controlling both the voltage, the electrical resistance of the TCA was effectively used to manipulate the displacement in real time. This self-sensing capability enables a streamlined control system, reducing the need for external sensors and enhancing the compactness of the overall design.

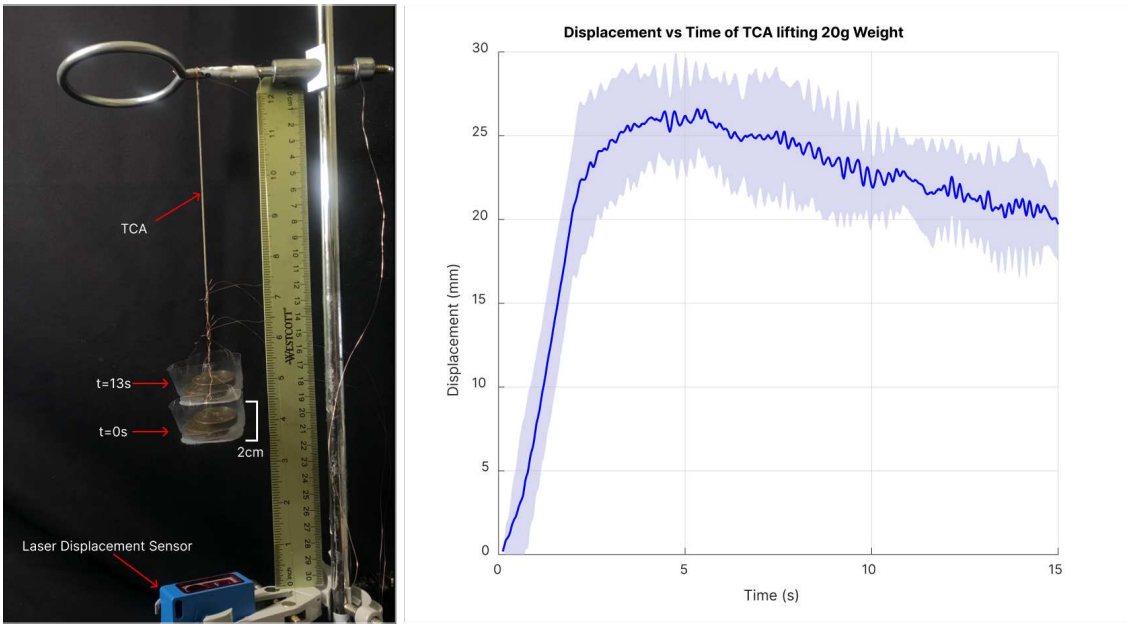


**Figure 2.6:** Experimental setup of closed loop control of TCA (left). The laser displacement sensor is used for validation of closed loop control to measure change in displacement during actuation. Graph of Displacement vs Time (right) of TCA during actuation. The set-point of experiments was 20 mm while lifting 20 g of weight.

We implemented closed-loop control of the bending angle by utilizing the self-sensing capability of TCAs, where the TCA's electrical resistance changes relative to displacement, reflecting the module's bending angle. To achieve this, the relationship between the TCA's resistance and the bending angle was first measured during the morphing process under a constant voltage of 10 V (other voltages yield similar results). The resistance-angle relationship was then modeled using a third-order polynomial fit, which can be seen in Fig. 2.7A. Since the resistance increases monoton-

ically, the module can be morphed to the desired bending angle by regulating the TCA's resistance to the corresponding value.

A proportional-integral (PI) controller was employed to achieve a target angle of 140° within 10 seconds and maintain it by regulating the resistance to 21.2  during the spine's stiffening process. Compared to the open-loop method, the closed-loop control significantly improves performance, making the morphing process more than 10 times faster, as seen in Fig. 2.7B. This is evident when comparing the time it takes for the angle to enter a small tolerance range (±3°), after which the spine stiffens to lock the desired shape.

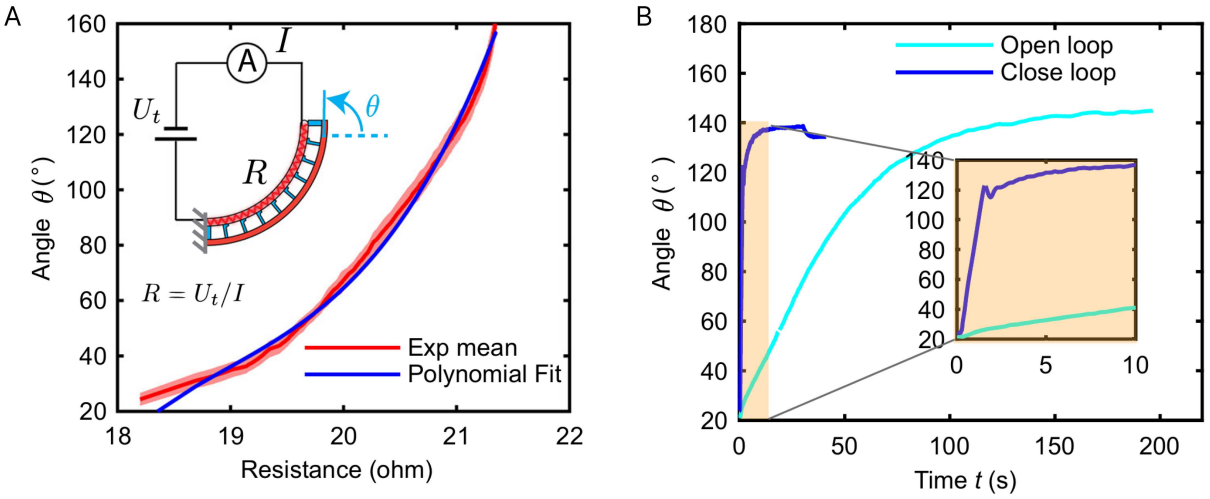


**Figure 2.7:** A) The experimental results demonstrate the relationship between the TCA's resistance and the module's bending angle, which is characterized by a third-order polynomial fit. B) A comparison was conducted between open-loop control, using a constant voltage of $U_t = 3V$ and closed-loop control, which utilizes resistance-based self-sensing. During the initial 10 seconds, the bending angle behavior is shown in the inset. The solid lines represent the average of three experiments, while shaded regions or error bars indicate one standard deviation from the mean.

## 2.4 Embedded Scheme Enables Various Other Shape-Morphing Modules

The embedded morphing scheme extends beyond simple 2D bending Shape Memory Materials (SMMs), offering advancements in two areas: 1) the ability to incorporate various types of defor-

mation strains (e.g., torsion) and 2) enabling more complex topologies (e.g., transitioning from a rod to a surface). To illustrate these extensions, a library of elementary SMM modules has been developed, including a twisting module, a 3D bending module, and a hybrid twisting and bending module.

Each module follows a consistent morphing strategy, which combines a Shape Memory Polymer (SMP) spine or base with sheathed Twisted Coil Actuators (TCAs). The SMP spine or base can adopt different geometries, while the TCAs are arranged in various patterns to achieve distinct deformation responses. For example, the twisting module can morph into a twisted shape around its axis, utilizing an SMP rod spine wrapped with resistance wire and a sheathed TCA, enabling up to 90° of twisting (45°/cm). This twisting module converts the linear actuation provided by the TCA and converts it to angular actuation by wrapping the sheathed TCA around a series of rings that are attached to the SMP rod. These rings are able to slide against one another, allowing for rotation between rings during actuation, as seen in Fig. 2.8A.

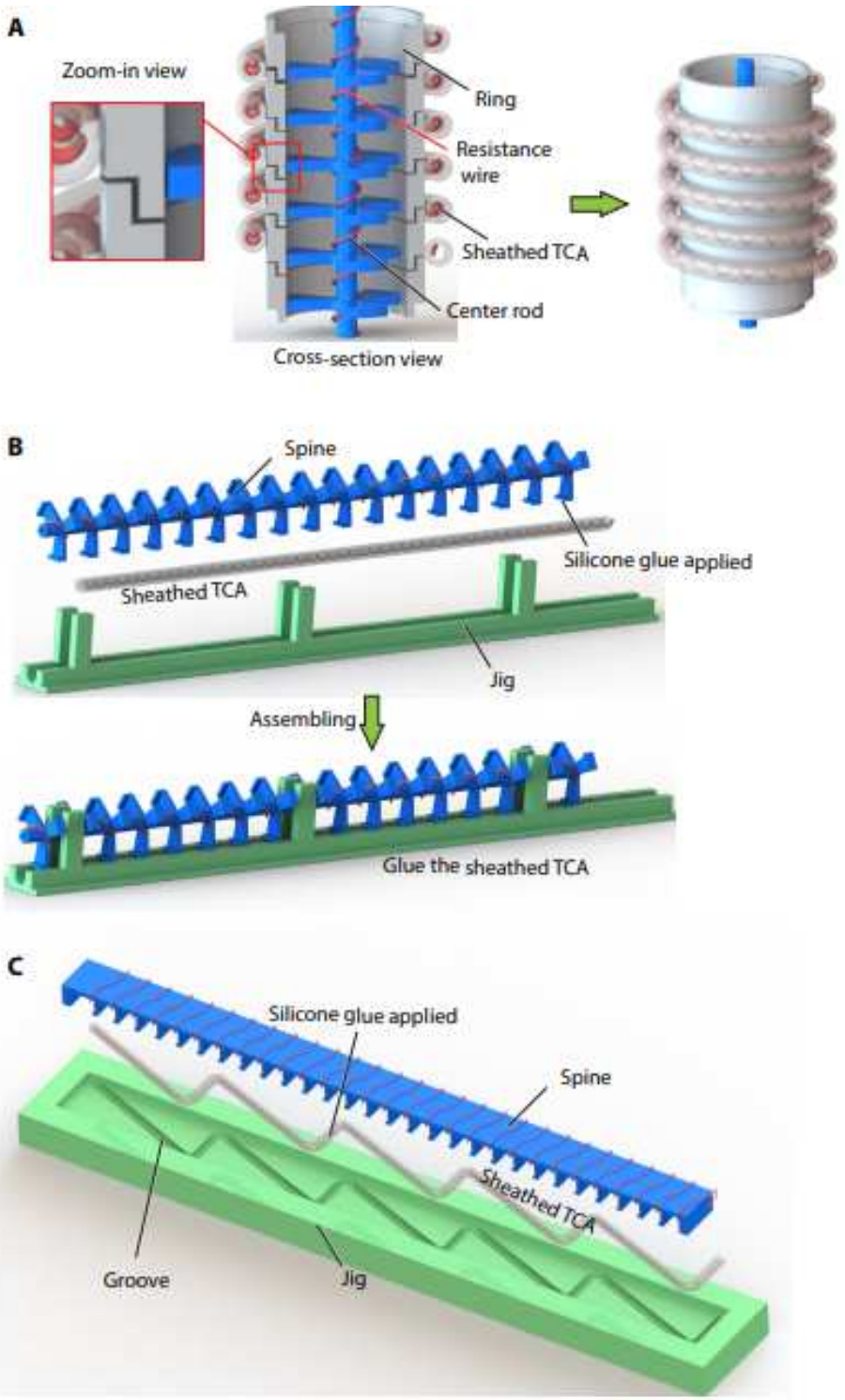


**Figure 2.8:** Design of the Twisting, 3D-Bending, and Combined Twisting and Bending Modules (A) The twisting module is constructed from several interlocking rings, allowing only rotational movement between neighboring rings, as shown in the zoomed-in view. (B) For the 3D-bending module, a jig is used to hold the TCA and the spine in a straight configuration during assembly. (C) To create the twisting and bending module, the TCA is fixed in a zigzag pattern using a jig and attached to the protrusions on the spine.

The 3D bending module employs an SMP rod spine with three rows of evenly distributed protrusions, with 3 sheathed TCAs attached in parallel, allowing for bending in 3 dimensions to any desired angle, shown in Fig. 2.9B. The hybrid twisting and bending module modifies the layout of the TCA on a larger SMP spine, creating sections of sheathed TCA that are attached at angle $\beta$ to the spine. This angle induces the regular bending motion, while also incorporating torsion to transform the bend into a helical shape, as shown in Fig. 2.9C.

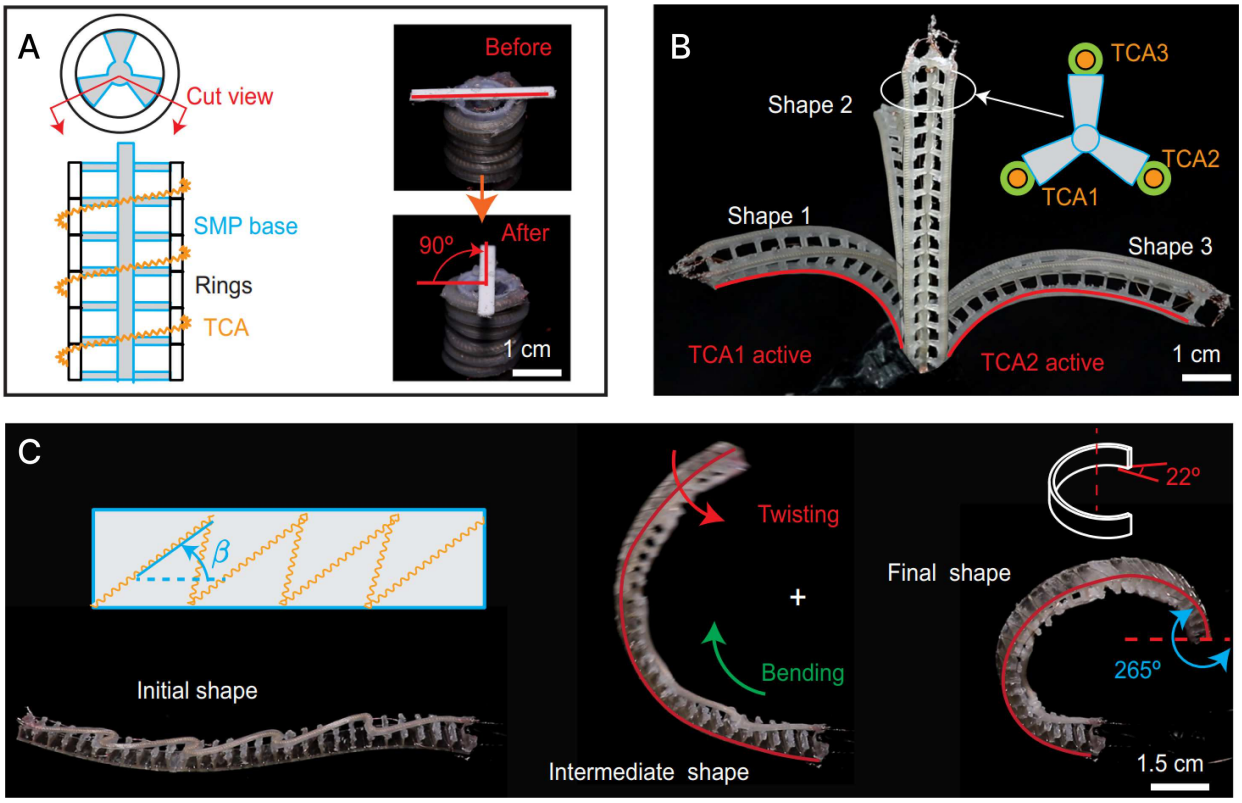


**Figure 2.9:** The embedded morphing scheme allows for the creation of various shape-morphing modules. A) The twisting module, featuring a sheathed TCA configured in a helical pattern, is capable of twisting up to 90° and maintaining that position. B) The 3D bending module utilizes three parallel sheathed TCAs, enabling it to morph into a wide range of 3D curved shapes. C) The twisting and bending module, with a sheathed TCA arranged in a zigzag configuration, can transform into a helical shape.

To showcase the portability of a SMM system in contrast to many other morphing robots, a system was developed using lightweight components paired with a SMM. The minimal system, which is comprised of a small, 11.1 V Li-Ion battery, micro controller (Arduino Pro Micro), and

motor driver (Pololu DRV8835), is all that is needed to control a SMM, all while fitting in the palm of the hand. Fig. 2.10 shows the compact nature of the minimal system.

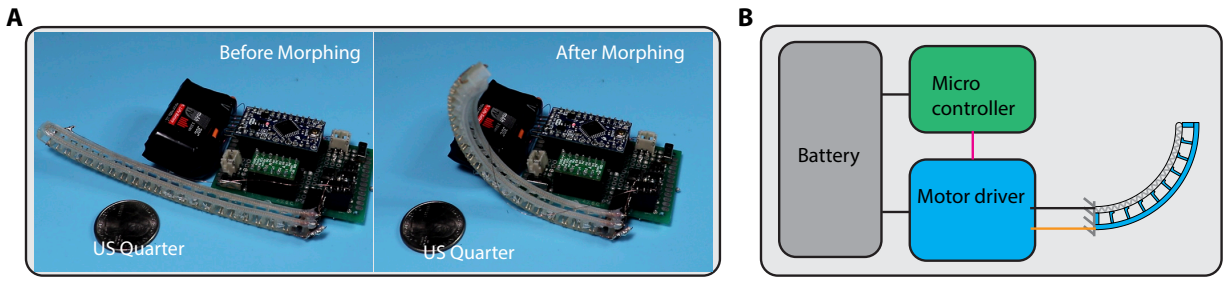


**Figure 2.10:** Minimal system utilizing SMM. The compact nature of the system compared to a quarter (left) and the driving components of the system (right).

## 2.5 Conclusion

The embedded morphing scheme presented in this section introduces a versatile and scalable approach to achieving complex deformations using SMMs. By embedding the actuation and control mechanisms directly into the material, the need for external morphing equipment is eliminated. The library of morphing modules developed—ranging from twisting and bending to surface morphing—illustrates the flexibility and potential of this scheme. This method offers a robust foundation for creating adaptive, reconfigurable systems that can perform in a wide range of applications, providing a new direction for embedded morphing technologies in fields requiring dynamic shape control.

# Chapter 3

# Robotic Fish with a Shape Morphing Tail

## 3.1 Introduction

Traditional robotic fish have been used in a wide array of applications, from surveying fish populations to inspecting underwater structures. These complex environments yield a desire for a robotic fish with high maneuverability and high speed. However, traditional robotic fish are normally limited to either swimming fast or being very maneuverable. Having a robotic fish with the ability to tune tail stiffness on the fly allows for this adaptability. Other robotic fish have tried to solve this problem, but the main issues are the mechanism required to tune the tail stiffness is large, complicated, or limited in capacity.

In this chapter, we will address the limitations of existing research to tune a fish's tail stiffness on the fly by using Twisted and Coiled Actuators (TCAs) combined with shape memory polymer (SMP). To stiffen the robotic fish tail on the fly, TCAs will be used to induce curvature into two thin plates on the tail. In literature, it has been found that applying transverse curvature to a thin plate has a dramatic increase in stiffness through the development of internal strains, increasing the elastic energy of the thin plate [41]. Depending on the distance of contraction of the TCAs, which can be controlled through self-sensing, a range of stiffness can be obtained for the tail. In conjunction with TCAs, shape-memory polymer is used to hold the thin plates in their position to lock the stiffness of the tail into place. We first detail the design of the robotic fish and its tail. We then discuss the characterization and experimental setup to understand the impact that controlling the curvature of thin plates on the tail has its stiffness. Then experiments were conducted to understand the impact of stiffness on swimming performance, focusing on straight-line swimming speed and maneuverability.

## 3.2 Design of Fish

The design of the fish takes inspiration from traditional fish, with an airfoil shape along the vertical profile, while maintaining ease of manufacturing using 3D printing. The body of the fish, shown in Fig. 3.1, is printed in two pieces and assembled. Inside of the fish's body is a low-density foam along the top of the body to maintain proper buoyancy, along with keep the fish oriented upright during swimming. The body of the fish also houses the servo motor, which is used to power the tail of the fish during swimming. Attached to the servo motor is the joint connector, which connects the tail of the fish to the servo motor. The tail, the most complication section of the fish, can be seen in Fig. 3.2, in which two thin plates on either side of the tail encase a modified variation of the SMM as described in Chapter 2.2. The thin plates of the tail are seated in a curved notch on the surface of the joint connector, which allows for a predetermined bias in regard to the bending direction of the thin plates. During initial testing, the plates were unreliable in their bending direction. The rear of the tail houses four SMP spines, running vertically along the tail, which are adhered to a thin plate, and connected to each other on the top and bottom of the fish via an elastic 3d printed connector. This elastic connector maintains the structure of the tail, while allowing flexibility during swimming. The elastic connector also doubles as an anchor point for the TCA.

As demonstrated in Chapter 2.4 with the minimal system, this entire system is capable of being run off of a small battery. However, it was determined that creating a waterproof, wireless robotic fish was not in the direct scope of this research, as many others have created wireless fish beforehand. Along with the amount of complexity that waterproofing electronic components such as this, it was decided early on that individual components would be waterproofed (servo motor, TCA, etc.), but the entire body would not be. Along with waterproofing most of the individual components, the shape morphing components had to be thermally insulated as well to allow for a thermal barrier between the cool water and higher temperatures of the morphing components. To accomplish this, dielectric grease was used to thermally insulate the modified SMMs. The main control circuit is separated from the fish, and is tethered to the rest of the components on the fish's

body. Many steps were taken to mitigate the impact of the fish being tethered during swimming, such as using the smallest, stranded wire. Along with this, ample length (1.5 m) was added to the tether to ensure no external forces were added during experiments. The driving principle of

**Figure 3.1:** Robotic fish with shape morphing tail.

stiffness variation is utilizing the modified SMM to induce curvature onto both thin plates in the tail. A great example of this stiffness change is taking a sheet of paper and applying curvature to one of the edges. Initially, the piece of paper is flat and has a very low stiffness, but once the curvature is applied, the stiffness increases. Also, the stiffness is also dependent on the amount of curvature applied to the thin plate. The curvature of the thin plates is a fundamental component in the tail's ability to adjust stiffness. When the thin plates curve, they undergo significant changes in their internal strain distribution, which directly affects the elastic energy stored in the system. This change in stored energy increases the overall stiffness of the tail, allowing for greater control over its mechanical properties. The interaction between the plates, the TCAs, and the SMP ribs is carefully coordinated to ensure that the tail achieves a wide range of stiffness on demand.

**Controlling Curvature via TCA Actuation.** The precise control of plate curvature is achieved through the self-sensing capabilities of the TCAs. As the TCAs contract, the degree of curvature is directly correlated with the displacement of the actuators. The self-sensing feature of the TCAs

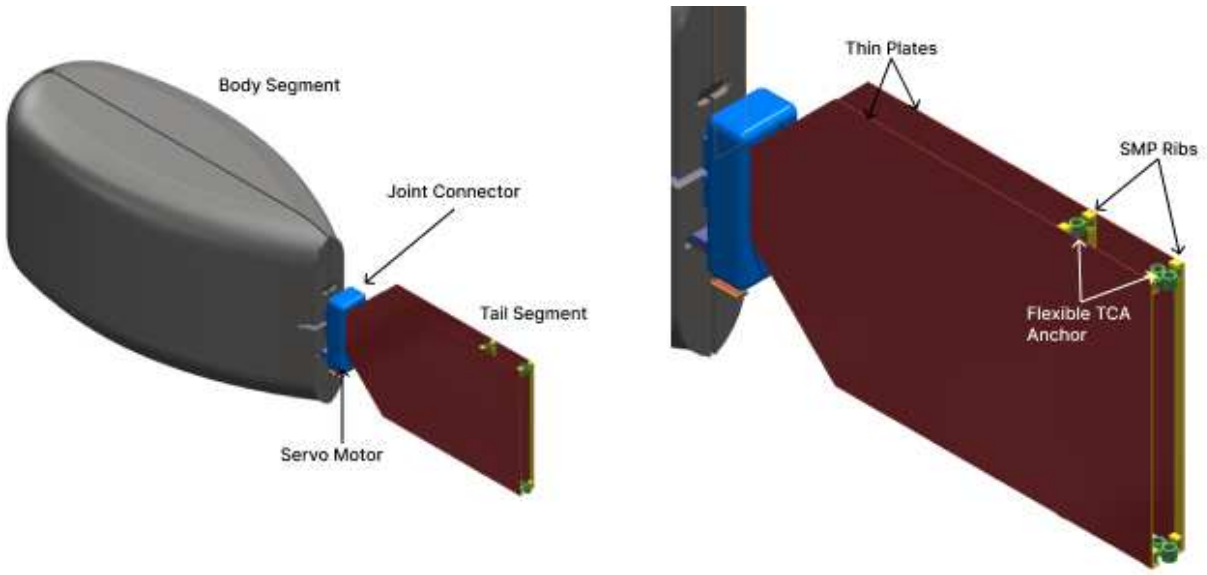


**Figure 3.2:** 3D model of the robotic fish with a shape-morphing tail, showing the body and tail segments. The tail segment is connected to the body via a joint connector and is actuated by a servo motor, enabling the tail to adapt its shape to different environmental conditions (left). Close-up of the shape-morphing tail section, showing the thin plates, SMP (Shape Memory Polymer) ribs, and the flexible TCA (Twisted and Coiled Actuator) anchor. The TCAs are attached to the flexible anchor, allowing the tail structure to morph in response to different environmental conditions (right).

allows for real-time monitoring of their displacement, enabling precise control over how much the plates curve.


**Figure 3.3:** Morphing sequence of the shape-morphing tail. In the initial flat configuration, the tail has low stiffness. As TCA actuation curves the plates, stiffness increases, with the curved shape held in place by the SMP ribs. During the recovery sequence, as the SMP returns to its original state, the stiffness decreases.

This closed-loop control system continuously adjusts the input to the TCAs based on feedback from their self-sensing mechanism. By measuring the change in electrical resistance during contraction, the system can accurately calculate the corresponding displacement of the TCAs. This

displacement data is then used to control the curvature of the plates, ensuring that the tail reaches the desired stiffness. The ability to finely adjust the plate curvature allows for real-time modulation of stiffness, making the tail highly adaptable to different swimming modes or conditions. This system does have limitations, however, as the force required to curve the thin plates does not remain constant during the bending process, which poses an issue for the reliability of the closed loop control, especially towards the upper limit of actuation distances and amount of curvature.

**SMP Ribs: Maintaining Curvature** The SMP ribs play a supportive role in maintaining the curvature once the desired shape is achieved. After the TCAs curve the plates to a specific shape, the SMP ribs ensure that this shape is locked in place. By heating the SMP ribs to their glass transition temperature, they soften and allow the plates to be morphed. Once cooled, the SMP ribs become rigid, holding the plates in their curved position and maintaining the stiffness generated by the curvature.

The ability to lock the plates in a curved state without continuous energy input makes this design particularly efficient. By relying on the intrinsic material properties of the SMP and the elastic energy stored in the plates, the system can maintain the desired stiffness passively, only requiring energy when stiffness adjustments are necessary. The recovery sequence of this particular system, shown in Fig. 3.3, utilizes the intrinsic properties of the SMP to recover to its flat shape, as well as utilize the stored internal energy from the bent plate to return to its initial shape.

## 3.3 Characterizations of the Developed Robotic Fish

Once the fish tail was constructed, a series of experiments were conducted to validate the effectiveness of the proposed mechanism in modulating stiffness. The actuation length of the TCAs directly correlates to varying amounts of curvature in the thin plates, which influences the stiffness of the tail. To test this, a series of actuation distances of the TCA were induced on the thin plates and held in place by the SMP ribs. Using a Mark-10 Series ESM303 Force Tester, force and displacement at the end of the tail were measured for different levels of TCA actuation, as seen in

**Table 3.1:** TCA actuation distances versus measured stiffness of pre-buckled and post-buckled state tail. Pre-buckled refers to the state of the tail during smaller end displacements (< 20 mm) and post-buckled refers to the state of the tail after at least one of the curved thin plates has buckled (>20 mm).

| TCA Actuation Distance (mm) | Average Pre-Buckled Stiffness ($10^{-3}$N*mm$^{-1}$) | Average Post-Buckled Stiffness ($10^{-3}$N*mm$^{-1}$) |
|---|---|---|
| Initial (0mm) | 7 | 1 |
| 1mm | 10 | 1 |
| 3mm | 10 | 1 |
| 5mm | 12 | 2 |
| 7mm | 15 | 3 |

Fig. 3.4. The initial stiffness (plates flat) as well as actuation distances of 1 mm, 3 mm, 5 mm, and 7 mm were tested. During experimentation, as well as during real world testing of the tail at relatively large displacements (approximately 20-25 mm), the tail entered a buckled state, in which caused the stiffness of the tail to decrease dramatically.

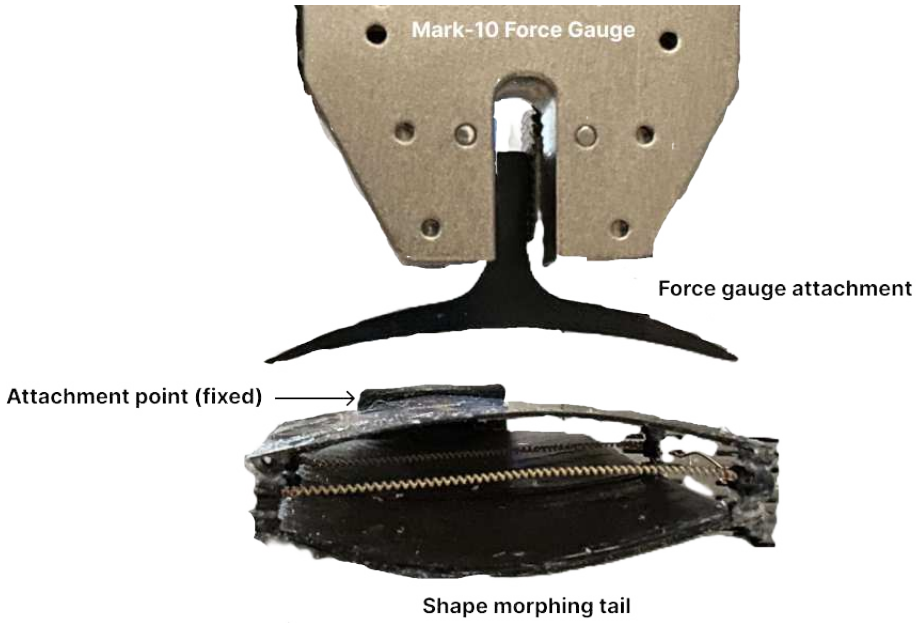


**Figure 3.4:** Experimental setup of stiffness experiments of the shape morphing tail. The attachment point used to connect to the fish is fixed, and the end of the tail is pushed vertically downward by the Mark-10 force gauge with it's attachment. The force and displacement are then recorded to obtain the stiffness.

The data reveal a clear trend: as the TCA actuation distance increases, curvature of the plates increases, so does the stiffness of the tail. This is evidenced by the increasing slope in the force-

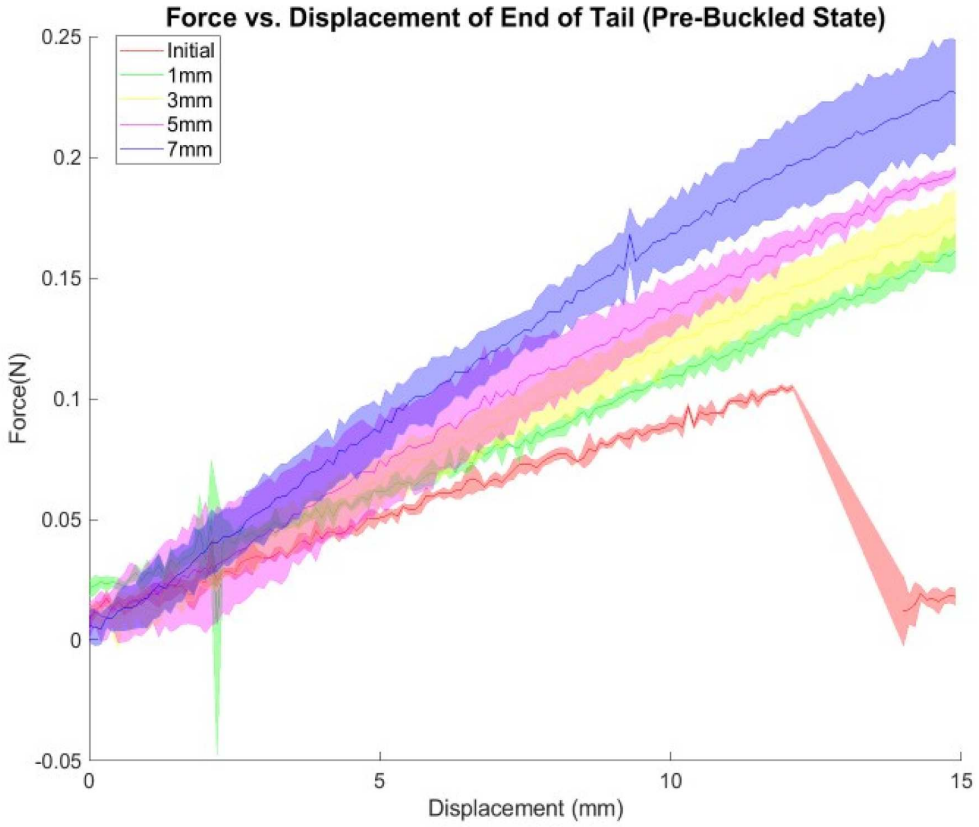


**Figure 3.5:** Force versus displacement of the tail's end in the pre-buckled state for varying TCA actuation distances. As the actuation distance increases (1 mm, 3 mm, 5 mm, and 7 mm), the curvature of the thin plates rises, leading to higher internal elastic energy and increased stiffness.

displacement graph during the pre-buckling state. The increase in stiffness with greater curvature is consistent with the theoretical model of elastic energy storage within the plates, as discussed previously. However, at very large displacements, the tail reaches a critical point where the thin plates buckle. This buckling results in a drastic reduction in stiffness, represented by a sharp drop in the slope of the force-displacement curve in the post-buckling state.

The buckling behavior is a crucial limitation of the current design. In the initial tests, the tail consistently buckled at a similar displacement, indicating that there is a threshold beyond which the thin plates can no longer maintain their structural integrity. This premature buckling is largely due to the relatively low initial stiffness of the tail in its flat configuration, which was designed to support flexible, fish-like swimming movements. While this flexibility is advantageous for

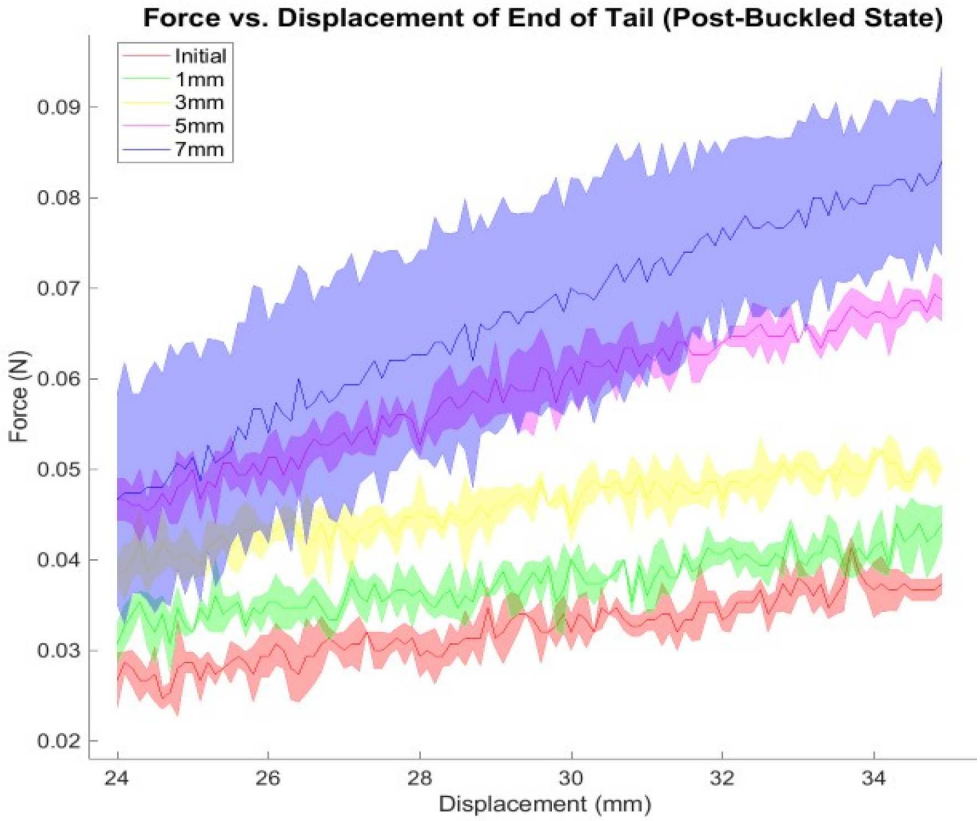


**Figure 3.6:** Force versus displacement of the tail's end in the post-buckled state for varying TCA actuation distances. The higher TCA actuation distances (1 mm, 3 mm, 5 mm, and 7 mm) lead to greater tail stiffness, as shown by the increase in force with displacement after buckling.

swimming, it presents challenges when attempting to achieve very high stiffness through extreme curvature.

Despite this limitation, the experiments successfully validated the tail's ability to modulate stiffness as expected. The pre-buckling data show a strong correlation between increased curvature and increased stiffness, proving the viability of the tail's design. Additionally, the results were consistent across trials, reinforcing the reliability of the stiffness modulation mechanism. However, a notable source of error was observed in the 7 mm actuation case, where the curvature achieved by the TCAs was difficult to maintain. This suggests that the current configuration of TCAs may not provide sufficient force to achieve higher levels of curvature without risk of buckling.

To further increase stiffness beyond the current limits, additional TCAs could be integrated into the system. By distributing the force more evenly across the tail, the plates could achieve greater displacement and curvature without reaching the critical buckling point. This modification would allow for more precise control over the stiffness, especially in applications requiring higher rigidity.

Overall, these experiments not only confirmed the capability of the tail to modulate stiffness based on curvature but also highlighted the limitations of the current design when subjected to extreme displacements. Moving forward, optimizing the TCA configuration and potentially adjusting the thickness of the thin plates could help mitigate the risk of buckling while increasing the tail's stiffness range would be the next steps.

**Effect of Stiffness on Swimming Speed and Maneuverability** To evaluate the effect of tail stiffness on swimming performance, a series of swimming tests were conducted, varying the stiffness of the tail by controlling the curvature of the thin plates. The swimming speed and maneuverability were recorded at different stiffness levels, providing insight into how stiffness influences the overall swimming dynamics of the fish.

The experiments reveal a trade-off between stiffness and swimming speed. At a constant actuation frequency (1.5 Hz), increasing the stiffness of the tail leads to slower swimming speeds. This reduction in speed is likely due to the decrease in the amount of generated thrust for the tested fre-

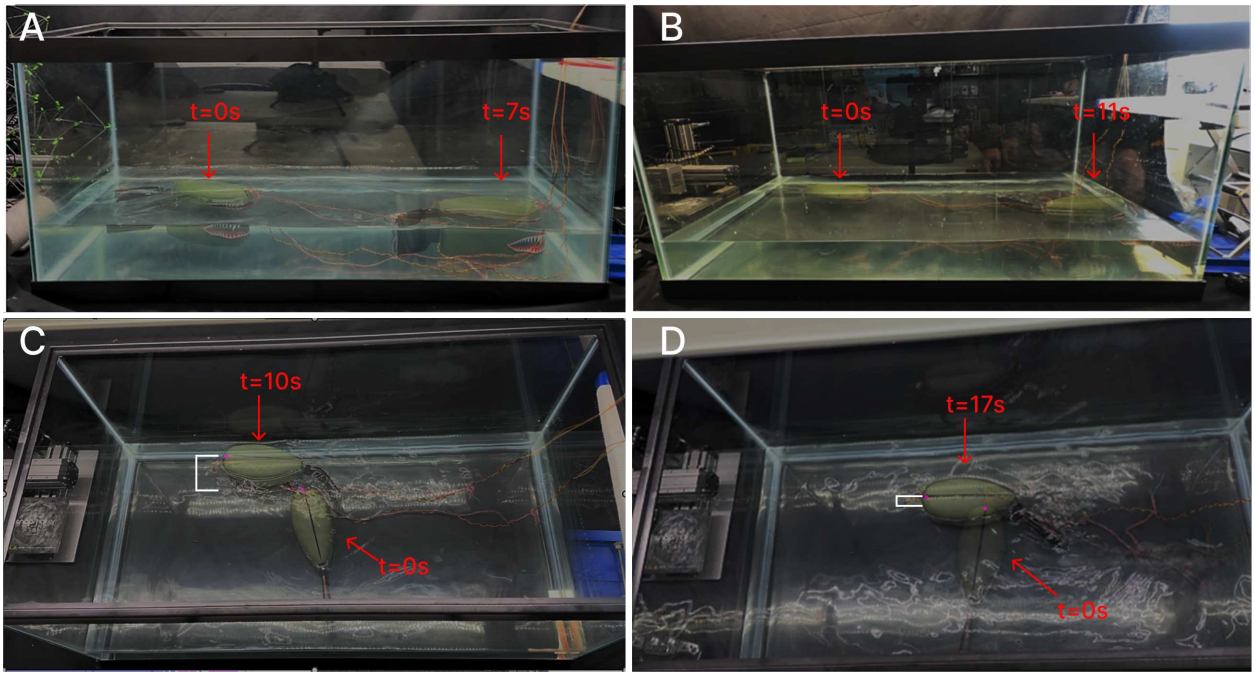


**Figure 3.7:** Effects of stiffness variation on forward swimming and turning at a frequency of 1 Hz. (A) Lower stiffness enables faster forward swimming, covering the same distance in less time (7 seconds) compared to (B) higher stiffness, which takes 11 seconds. (C) Initial stiffness results in a wider turning radius, as shown at 10 seconds, while (D) higher stiffness decreases the turning radius at 17 seconds.

quency. However, the trade-off comes with a significant improvement in maneuverability. A stiffer tail allows the fish to execute more precise and controlled movements, making it better suited for tasks that require sharp turns or complex navigation.

This relationship between stiffness and performance aligns with findings in other literature, which suggest that stiffer tails provide more controlled motion, making the fish more agile and responsive. However, in instances where the frequency becomes higher, stiffer tails tend to provide more thrust and thus swim faster.

**Impact of Frequency on Performance and Buckling Limitation** At very large frequencies (e.g., 2.5 Hz), the forces acting on the tail become too great for the structure to handle, leading to buckling. The buckling of the thin plates significantly reduces stiffness and, as a result, the swimming efficiency decreases. Figure 3.8 highlights this limitation, showing the process of inducing a large force on the end of the tail that allows the tail to buckle. This buckling phenomenon limits

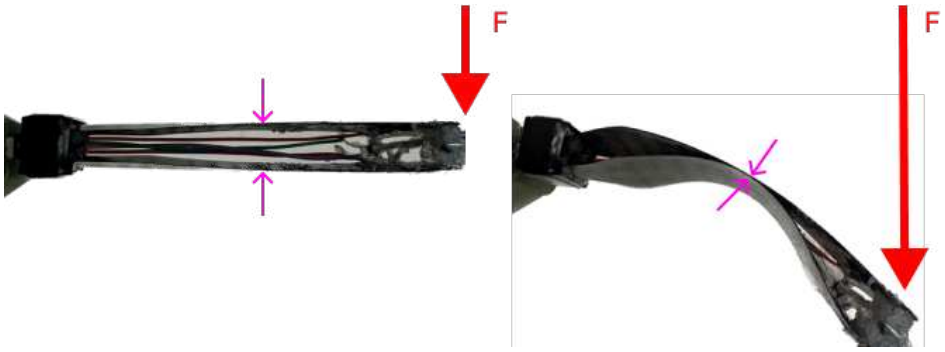


**Figure 3.8:** At high frequencies (>2.5 Hz), the thin plates experience buckling, leading to a significant decrease in stiffness and instability during swimming. This reduces propulsion efficiency due to the loss of structural integrity.

the maximum frequency at which the fish can swim effectively with a stiffer tail. The forces generated at high frequencies exceed the structural capacity of the tail, causing instability and reducing the overall propulsion efficiency. As a result, future iterations of the tail design may require reinforcement or additional actuation mechanisms to overcome this limitation and extend the usable frequency range without inducing buckling.

## 3.4 Conclusion

In this chapter, a mechanism to change the stiffness of a robotic fish's tail using a combined morphing strategy using TCAs and shape memory polymer is presented. By using the TCAs to precisely actuate and control the curvature of two thin plates within the tail, a wide range of stiffness can be achieved. This range of stiffness can then be used to optimize the performance of the robotic fish with respect to the tail frequency to maximize both speed and maneuverability. Compared to traditional robotic fish with only one tail stiffness, the advantage of adapting to different environments provides a compelling argument. This is especially the case against other variable stiffness mechanisms used to change tail stiffness, in which this is one of the only options that can be implemented in small form-factor, fully wireless robotic fish.

# Chapter 4

# Robotic Fish with a Shape Morphing Body

## 4.1 Introduction

As mentioned in earlier sections, the shape of a fish's body can have tremendous impacts on swimming performance. By modifying different characteristics of a fish's body (length, body depth, body stiffness, etc.), a singular robotic fish has the ability to adapt to its environment by improving swimming performance. Many researchers have looked at stiffness as the main factor in affecting swimming performance.

What has yet to be investigated until now is how to modify the swimming performance of a robotic fish by changing the shape of its body to accomplish different swimming speeds and accelerations. The fish created and studied for this chapter utilizes additive manufacturing techniques with a modified version of the shape memory polymer ribs described in the previous chapters to accomplish the shape morphing design. The fish is propelled forward via 3 servo motors, and controlled using a Central Pattern Generator (CPG), a mathematical model, which excels particularity at undulatory and repetitive movement. By modifying input parameters to the CPG model, different characteristics of the output (frequency, amplitude, phase offset between motors) can be changed. This variations in swimming parameters will help directly compare different body shapes against each other to find an ideal combination of parameters to maximize swimming speed.

In this chapter, we will introduce the design of the robotic fish and the modifications made to the SMM to accommodate this new fish design. We then will introduce the Central Pattern Generation model utilized to control and coordinate swimming. We then introduce the methodology of body morphing utilized and its impact on swimming performance. The rest of the chapter will outline the experimental results of the fish swimming with different swimming parameters and body shapes.

## 4.2 Fish Body Design and Modification of SMM

The robotic fish consists of four main sections: the head, the first body section, the second body section, and the tail. These sections are controlled by three servo motors, positioned between each segment to manage the bending and undulatory movements, enabling lifelike swimming patterns.

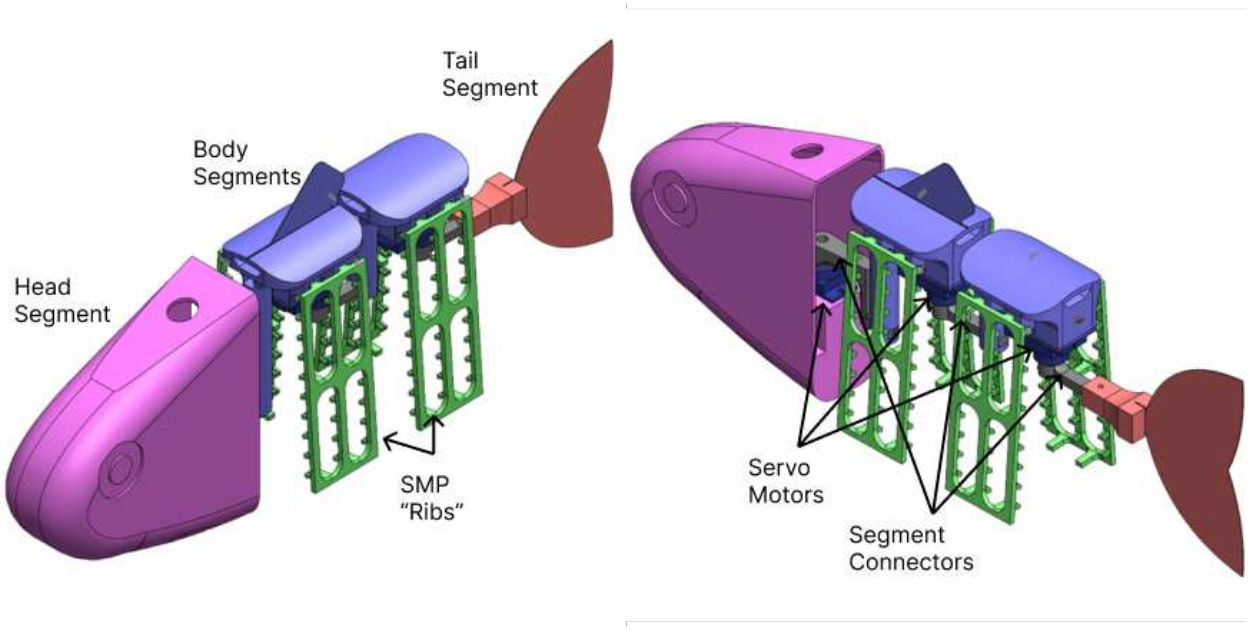


**Figure 4.1:** Solid Works model of the body-morphing fish, consisting of four segments: a head, two body segments, and a tail segment. Each segment is connected by joint connectors controlled by servo motors. SMP (Shape Memory Polymer) ribs are attached to the sides of the fish and can be actuated by TCAs (Twisted and Coiled Actuators) to change the shape of the fish.

Each body section is outfitted with a pair of modified shape morphing modules, as seen in Fig. 4.1. These modules have been tailored to fit the dimensions of the fish, with their width increased to maintain rigidity in underwater environments. This modification ensures that the fish remains both flexible and durable, capable of adjusting its shape dynamically to enhance maneuverability and energy efficiency. Another important modification is how each rib in comprised of three smaller, vertical, SMP spine, with it's own set of protrusions to attach 3 sheathed TCAs in parallel to increase the amount of force expected to morph against the outer silicone shell. The final modification is the addition of two larger protrusions along the top and bottom of the rib, which allow

for anchoring the rib to the body section, as well as utilize a rigid connector at the bottom of the rib to increase stability.

The entire fish body is encased in a soft silicone shell, providing a flexible and hydrodynamic outer layer that protects the internal components. This shell minimizes drag, allowing for smooth interaction with water, and shields the mechanical components from environmental damage. On the bottom of silicone shell is a re-closable faster that can be opened when needed to complete repairs on motors, remove the SMP ribs, or other maintenance that might be needed. Similar to the previously designed robotic fish, only the necessary components are waterproofed, including the motors. To obtain the proper buoyancy, a combination of low-density foam and weights were used.

All major components of the robotic fish, excluding the silicone outer shell and shape morphing modules, are 3D-printed. This choice of material offers both customization and lightweight design, which is critical for optimizing the fish's swimming performance. The use of 3D printing also facilitates quick adjustments and replacements during the design and testing phases, making the robotic fish adaptable for various experimental conditions. The ability to have complex designs, such as those of the body segments, would not have been possible with traditional manufacturing methods.

**Figure 4.2:** Body-morphing fish encased in a silicone skin to reduce drag during swimming. The bottom of the fish body can be opened to allow access to internal components.

To further reduce weight and enhance swimming efficiency, the fish is tethered to a microcontroller positioned outside its body. This external microcontroller provides real-time control over the motor outputs and behavior, ensuring precise coordination of movements while minimizing the load carried by the fish itself. Having the microcontroller outside of the body also reduces the complexity of waterproofing the fish.

In this design, TCAs were not directly integrated into this system, given the introduced complexities of having multiple motors, a new control model, and new SMM, the focus was understanding the impact that a morphing body could have on swimming. While directly integrating all of the components to morph the body shape on the fly is the ideal end-goal, it was decided to first tackle the design and incorporation of morphing-capable components before integrating on the fly morphing.

## 4.3 Central Pattern Generator

In robotic systems that require rhythmic motion, such as undulatory swimming, Central Pattern Generators (CPGs) are frequently employed to generate oscillatory motor outputs without the need for rhythmic external inputs. The CPG model utilized in this work was adapted from the framework described in previous research on fish-inspired robotic swimmers [8, 27]. Specifically, this model was originally implemented for controlling motor outputs in a serpentine robot. In adapting this model for our robotic fish, which uses three motors, the CPG outputs were modified to control motor actuation based on specific input parameters, impacting the swimming performance.

The CPG employed in our work is a dual-neuron model proposed by Wu et al. [8], where each motor is controlled by a CPG module. The modules consist of two neurons that inhibit each other, producing rhythmic outputs. These outputs control the actuation of the three motors in the robotic fish, with each motor corresponding to a different segment of the fish body, including the head, midsection, and tail. By adjusting the CPG parameters, such as frequency, phase difference, and intensity, the motor outputs can be fine-tuned to create different swimming behaviors.

In this model, $N$ represents the number of actuators (or CPG modules), and the dynamics of each module are governed by the following equations:

$$\tau_1 \dot{U}_{i,j} + U_{i,j} = E_i - \beta_i V_{i,j} - \alpha y_{i,3-j} + \omega y_{i-1,j}$$

$$\tau_2 \dot{V}_{i,j} + V_{i,j} = y_{i,j}$$

$$y_{i,j} = max(0, U_{i,j})$$

$$y_{i,out} = y_{i,1} - y_{i,2}$$

$$i = 1, 2, ..., N; j = 1, 2$$

where $U_{i,j}$ is the membrane potential of the $j$-th neuron in the $i$-th CPG module, $V_{i,j}$ is the inhibitory output of the neuron, $E_i$ is an external input (or external stimulus), $\beta_i$ is an adaptation coefficient for the module, $\alpha$ is the mutual inhibition weight between neurons within the module, $\omega$ is the inter-module connection weight, linking neuron $j$ of the $i$-th module with the preceding module. The output of the $i$-th CPG module is given by $y_{i,out}$, which is the difference between the outputs of its two neurons.

The rhythmic outputs of the CPG are characterized by their frequency, phase differences between modules, and intensity. Specifically, the time constants $\tau_1$ and $\tau_2$ determines the baseline frequency of the motors and the phase offset between motors is impacted by the difference between $\tau_1$ and $\tau_2$. In our experiments $\tau_1$ was held constant at 0.1 and $\tau_2$ was varied in order to reduce the number of independent variables. The inter-module connection weight $\beta$ has an impact on adjusting the frequency from the predetermined baseline as well as slightly impact the phase offset of the motors. The external input $E_i$ adjusts the intensity of the outputs. All other parameters remain fixed during operation. The next step taken was to determine the method of communicating the output of the CPG, which outputs an arbitrary number $y_{out}$, to a microcontroller to control the motors simultaneously. The method that was determined was to constrain the output of the CPG between -1 and 1. By doing this, the output of the CPG, which was ran on MATLAB, was sent

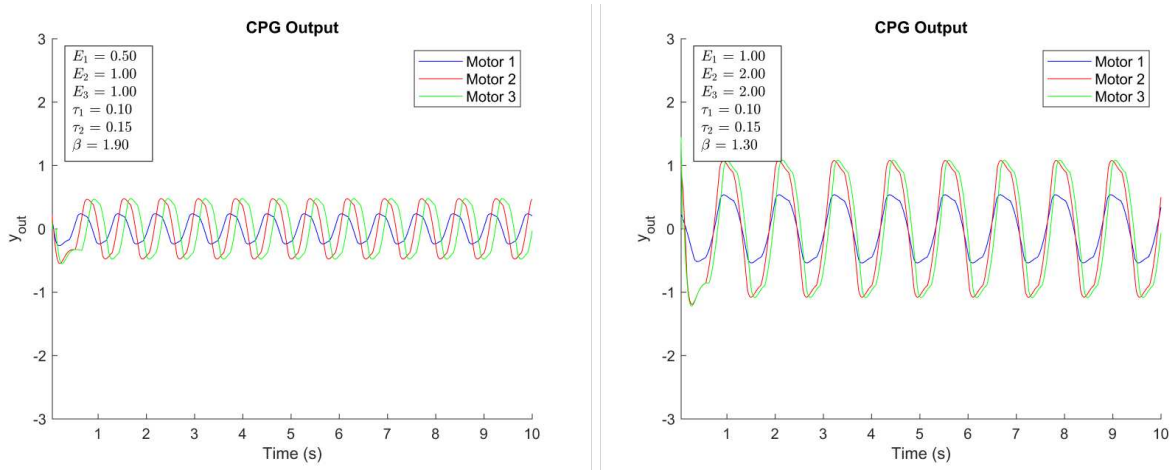


**Figure 4.3:** Central Pattern Generator (CPG) output for two different sets of input parameters. The CPG output (y_out) changes based on varying inputs of $\tau_1$, $\tau_2$ (time constants), $\beta$ (x), and $E_1, E_2, E_3$ (intensity constants of each motor). The y_out signal is synchronized with the Arduino, controlling the fish's servo motors, converting a y_out ratio of -1 to 1 into a servo angle range of 35 to 145 degrees.

via serial communication to an Arduino microcontroller. The microcontroller then read the value of the CPG of each motor, and map that value to an angle between 30 degrees and 150 degrees. These values were chosen as the extremes due to the physical rotational limits of the motors. Once the angle was mapped, it would then be coordinated to its respective motor for the duration of the swimming procedure.

The selection of range and magnitude of values tested for $\tau_2$, $\beta$, $E_1$,$E_2$, and $E_3$ was a combination of multiple factors. Given the selection of $\tau_1$=0.1, the difference between $\tau_1$ and $\tau_2$must provide a large enough phase offset to impact swimming, without having such a large phase offset that it has a negative impact on swimming. Thus, values of 0.01, 0.03, and 0.05 were chosen. The values of $\beta$ were also chosen to represent a range of motor frequencies that could mimic the frequency of biological fish cruising (0.5 Hz - 2 Hz). Given this range, as well as the physical limitation of the speed of the motors inside of the fish, values of $\beta$ = 1.0, 1.3, 1.6, and 1.9 were chosen to represent this range of frequencies. Given the constraints of $-1$ and 1 by $y_{out}$, finding a range of values was relatively simple for the values of $E$. It was decided after watching biological fish and referencing literature that the value of $E_1$ would be exactly halved in comparison to $E_2$ and $E_3$. While referencing fish swim, it was noted that a fish head's amplitude was significantly

smaller in comparison to the rest of its body. Thus, it was concluded that $E_1$ must be significantly smaller to reflect this. Thus, the values selected for [$E_1$, $E_2$, $E_3$] are [0.5, 1, 1], [0.75, 1.5, 1.5], and [1, 2, 2]. In the current configuration of the CPG, a value of $E_2$ and $E_3$ = 2 yield a magnitude of $y_{out}$ equal to 1.

## 4.4 Body Shape Morphing and Its Impact on Swimming Performance

The shape of a fish's body can have a tremendous impact on its swimming performance. From a fluid dynamics perspective, a fish with the lowest amount of drag will have to overcome the least amount of hydrodynamic forces, allowing for faster swimming. However, a fish with a deeper body is able to have more stability during maneuvering. Having these trade offs with respect to body shape shows the necessity of a robotic fish that can change the shape of its body. By the intrinsic nature of the morphing modules used in the fish, It can be seen in Fig. 4.4 that when the SMM ribs are morphed, both the vertical height of the module changes, as well adding additional width to the body of the fish. This combination of adjusting both body depth and width simultaneously is both novel and unique to our work.

To understand what shape the modules should be morphed into to have the largest impact on swimming, we must first look at biological inspiration. When looking at cruiser fish's vertical profile, such as tuna, their shape closely resembles that of an airfoil. However, looking at a bluegill, their body vertical profile is nearly flat for the entire length of the body. To reflect these different body shapes, maintaining a flat profile along the length of the robotic fish's body, such that both modules are flat, was chosen as the first body shape. This body shape, designated during testing as flat-flat (FF) body shape, was the first shape tested. This shape correlates to the morphing ribs of the fish in their un-morphed length, $L_0$. Looking next at a tuna-like profile, we looked at what the physical limits of morphing could accomplish with respect to what a TCA would be able to displace in its current configuration. Similar to the previous fish stated in Chapter 3, 7 mm of actuation distance was chose for the front pair of ribs, and 3 mm was chosen for the rear pair of

ribs. This combination of medium and large rib shapes were denoted as medium-large (ML) body shape. As seen in 4.4, the vertical profile of the ML body shape somewhat resembles an airfoil shape.

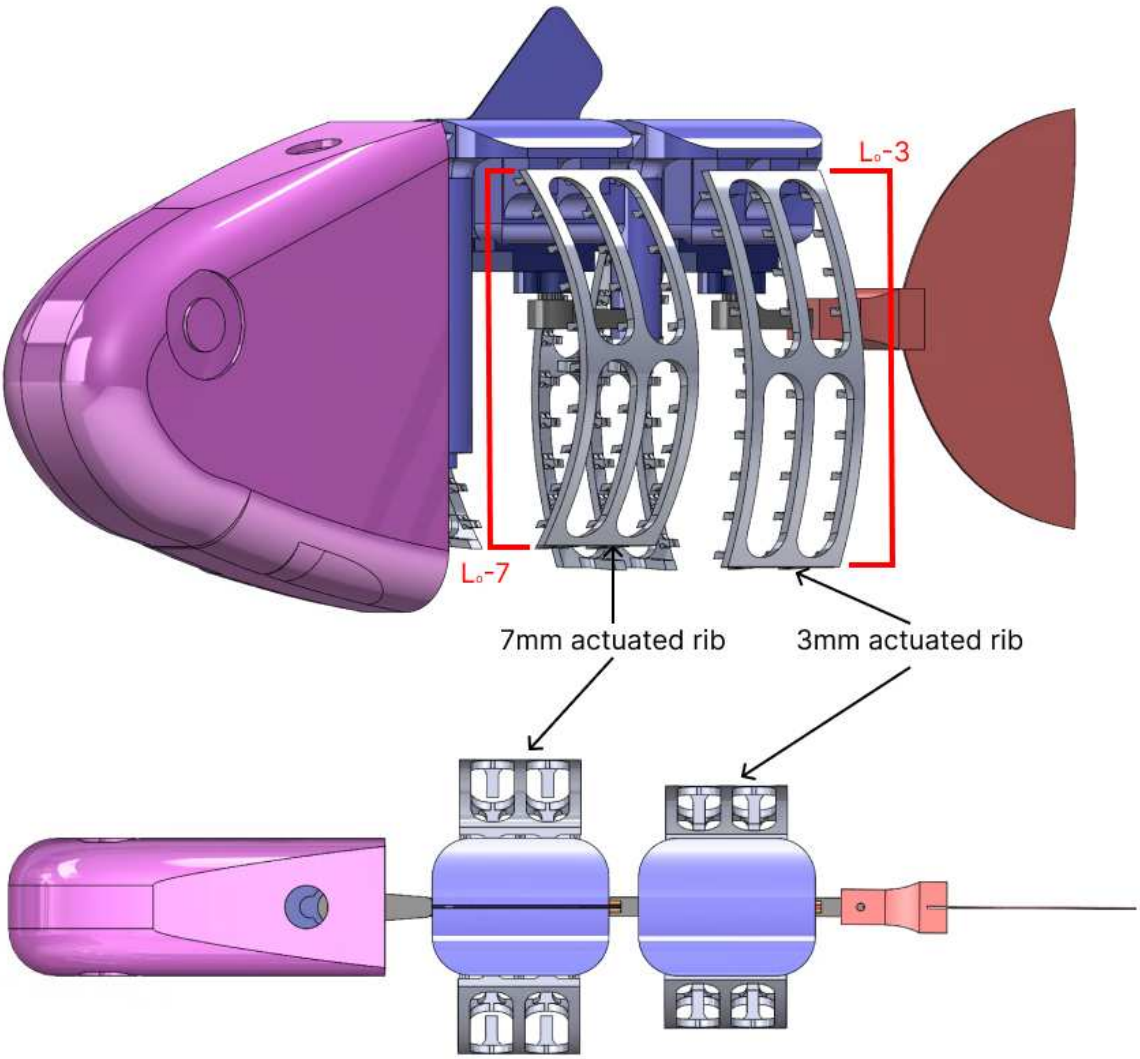


**Figure 4.4:** Solid model showing ribs actuated by varying TCA displacements to create a distinctive body shape. This body shape, referred to as medium-large (ML) shows an actuation distance of 3 mm (medium) and 7 mm (large). The shape of the body is made to imitate an airfoil shape seen in some biological fish.

Since TCAs have not been directly integrated into the shape morphing system, the ribs must be removed from the body to be morphed into the proper shape and reinstalled before swimming. Although not ideal, this system still provides the same swimming results compared to a system with integrated TCAs. However, this system is perfectly prepared to accommodate TCAs into the system, with the proper protrusions on the SMP ribs, as well as cable routing channels to actuate the TCAs.

## 4.5 Optimal Speed Analysis for Different Body Shapes

Experiments were conducted to analyze the impact of different body shapes had on swimming performance. Using a USB webcam (EMEET Smartcam S800, 4k) mounted directly over the center of the pool, videos were taken and analyzed using Tracker software. The experimental setup can be seen in Fig. 4.5, where a ruler was placed in the water to properly scale the video. The pool, sized 60 inches in diameter and 12 inches deep, was deemed sufficiently large enough as to not impact performance due to waves bouncing off the walls. The pool was filled approximately to 10 inches in depth, as to provide ample clearance so the fish would not touch the bottom of the pool during swimming.

At the start of each experimental run, the fish would be placed in the tank at a sufficiently far enough distance away from the wall of the pool to mitigate any external effects. Once the fish was plated and oriented in the correct direction (running vertically through the center of the pool), the CPG model would be ran for the unique set of parameters chosen for the given run, and the fish would swim for 10 seconds, regardless of the parameters used. At the end of the 10 second run, the fish would be moved back to its original starting point, the CPG parameters would change, and the process was repeated until all chosen combinations of CPG parameters were used for both FF and ML body shapes.

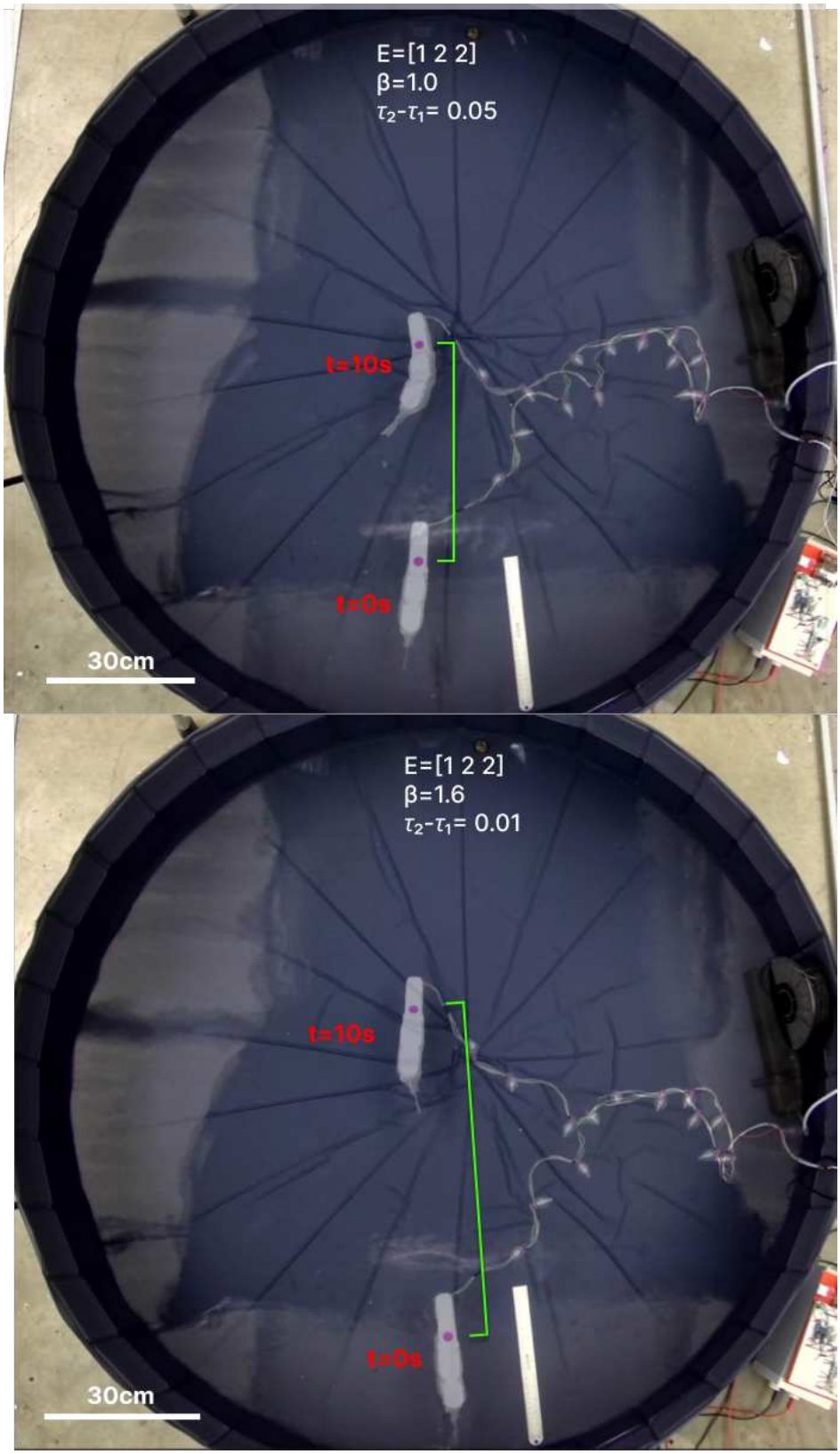


**Figure 4.5:** Body- morphing fish swimming. With the same body shape, altering other parameters such as $\beta$, $E$, and $\tau_2 - \tau_1$, results in significant changed in swimming speed, as shown over a 10- second interval.

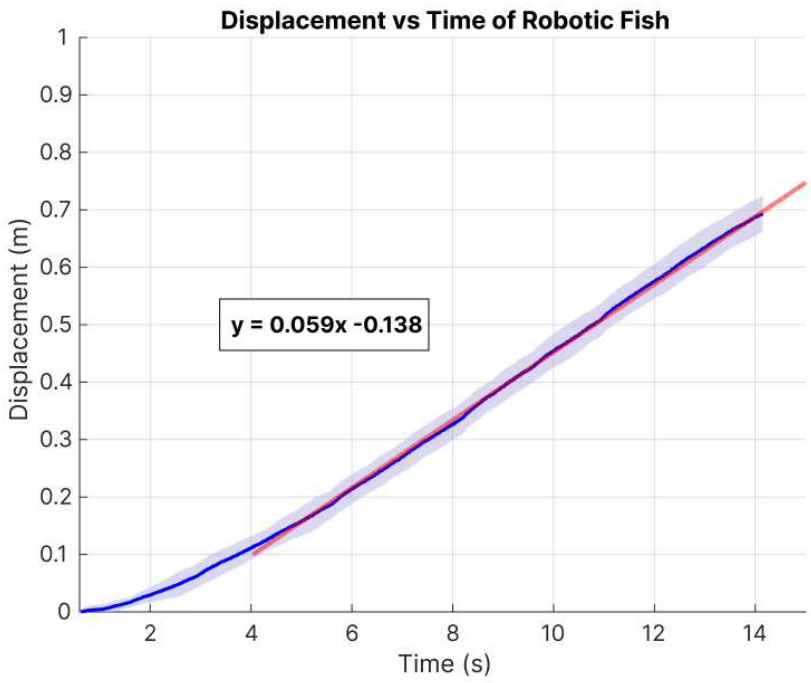


**Figure 4.6:** Illustration of how the steady-state swimming speed is extracted from experimental data. Displacement vs. Time of robotic fish during swimming experiments using parameters $E$=[0.5 1 1], $\tau_2$ - $\tau_1$=0.03, $\beta$=1.6, and FF body shape. A trend line was used to calculate average swimming velocity once the fish reached steady state velocity.

Using tracker software, the forward swimming velocity was calculated from the point the fish reach a constant swimming velocity (approximately >4 seconds), as seen in Fig. 4.6. In doing so, the effects of the fish accelerating from a stop was neglected. The final results can be seen in Fig. 4.7, where a series of 6 grids shows the data in heat-map form. Each grid corresponds to a series of experiments that use the same set of $E$ values. Along the vertical axis of each grid is the $\beta$ values, and the horizontal axis is the differences between $\tau_2$ and $\tau_1$. The 3 grids in the top row all correspond to the FF body shape, and the bottom row of grids correspond to the ML body shape. Speed is represented by the color of the square within any given grid, represented as a scale. The closer to green, the faster the fish is given the set of parameters and body shapes used. The results in Fig. 4.7 show the impact and function of body shape in combination with CPG parameters. When looking at values with the highest swimming speed, it can be seen that there is an optimal combination of values to achieve the highest swimming speed. When looking at each grid

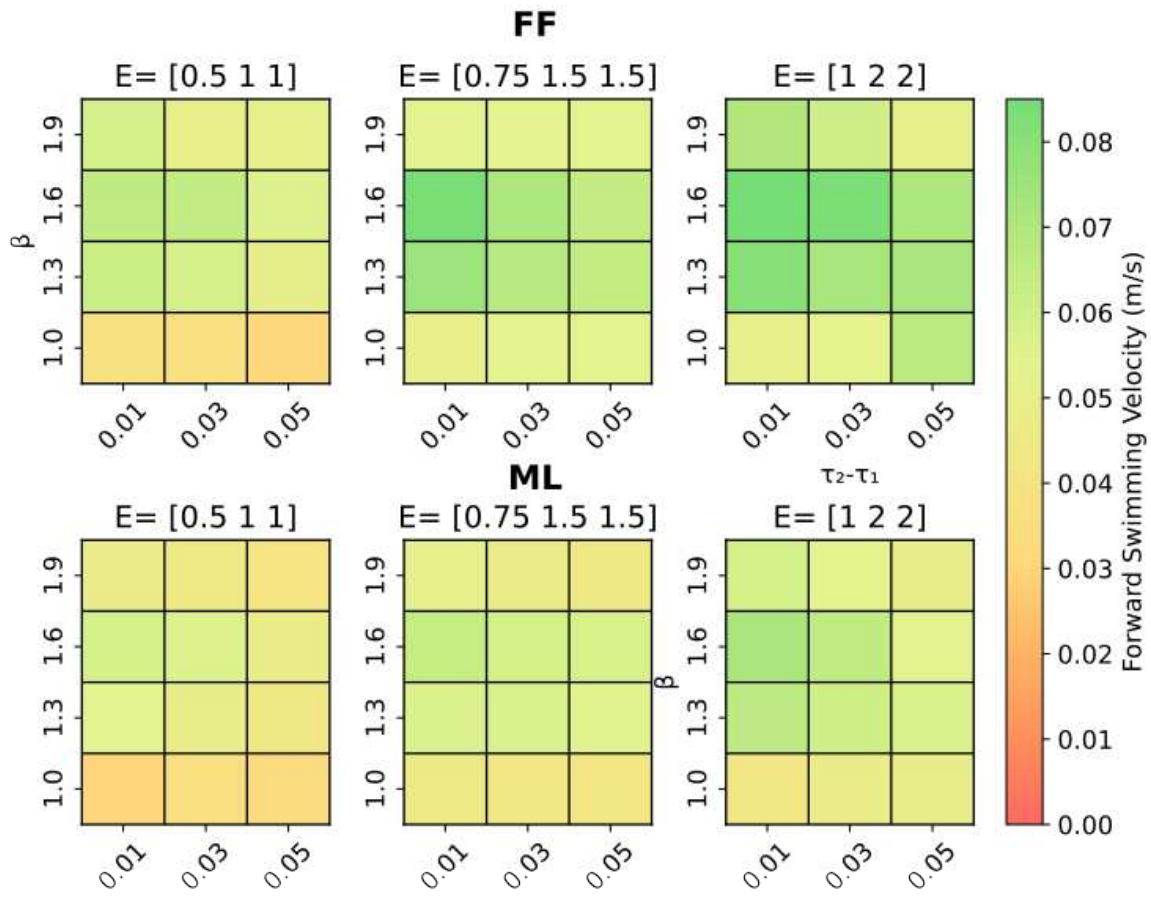


**Figure 4.7:** Heat maps showing forward swimming velocity (m/s) as a function of $\beta$ and $\tau_2 - \tau_1$ for different values of $E$. The top row (FF) represents forward swimming with a flat-flat body configuration, while the bottom row (ML) shows a medium-large body configuration.

and comparing the swimming speed values to $\beta$, it shows the optimal values to obtain the fastest swimming speed is in the range of $\beta$ equal to 1.3-1.6, with diminishing returns at both 1.0 and 1.9. Also, having the lowest difference between $\tau_2$ and $\tau_1$ proved to yield the fastest swimming speed for each case. As expected, increasing the amplitude also showed increase in swimming speed.

In all conditions, the FF body shape outperformed the ML body shape in forward swimming velocity. After further examination, it is most likely due to a few factors. The driving principle of having testing the ML body shape was to examine a body shape that closely resembles that of an airfoil. However, while looking at the vertical profile of the fish in Fig. 4.4, the rigid fish head stays the same width regardless of body shape. This sharp change from the width of the fish head

to the large width induced by the first set of morphed ribs most likely introduced unexpected drag in the setup. With increased drag, this yielded slower swimming speeds. One design change that could be implemented would be to add an additional set of shape morphing ribs inside of the head and extend the soft silicone shell. By adding an additional set of ribs, the opportunity to test more body shapes, as well as have more streamlined shapes.

## 4.6 Conclusion

In this chapter, we demonstrated the design and testing of a robotic fish capable of body shape morphing to explore its effects on swimming performance. By employing additive manufacturing techniques and integrating modified shape morphing modules (SMM), we successfully created a fish with adaptable body configurations. Experimental results revealed that body shape significantly influences swimming velocity, with the flat-flat (FF) configuration consistently outperforming the medium-large (ML) configuration due to reduced drag and a more streamlined profile.

Utilizing a Central Pattern Generator (CPG) model allowed precise control of swimming dynamics by varying key parameters such as frequency, phase offset, and intensity. Our analysis showed that optimal swimming speeds were achieved with intermediate values of $\beta$ (1.3–1.6) and minimal phase offsets ($\tau_2$-$\tau_1$). However, the ML configuration's performance was hindered by design limitations, including abrupt transitions in body width that increased drag. These findings highlight the importance of holistic body design when evaluating morphing capabilities.

Future iterations could address these limitations by incorporating additional morphing modules in the fish head and extending the silicone shell for smoother transitions. This would enable testing of more streamlined body shapes and further validate the potential of dynamic shape morphing to optimize swimming performance. The demonstrated ability to tune body shape and swimming parameters paves the way for versatile robotic systems capable of adapting to diverse aquatic environments.

# Chapter 5

# Conclusions and Future Work

## 5.1 Conclusions

This thesis explored the development of robotic fish with advanced shape-morphing capabilities to enhance adaptability and swimming performance. The integration of Shape Morphing Modules (SMMs) with Twisted and Coiled Actuators (TCAs) enabled dynamic tuning of stiffness and body configurations, paving the way for robotic systems that mimic biological locomotion in diverse aquatic environments.

The embedded morphing scheme introduced in this research represents a scalable and versatile approach to achieving complex deformations, such as bending, twisting, and surface morphing. By incorporating actuation, sensing, and shape-locking mechanisms directly into the robot's structure, this method eliminates the need for external hardware, making it a compact and efficient solution. The success of these modules was demonstrated across a range of applications, including adaptive grasping and dynamic body morphing, illustrating their potential for broader use in soft robotics and other fields.

The study of the robotic fish's tunable tail provided key insights into the trade-offs between speed and maneuverability. Experiments demonstrated that increasing tail stiffness enhanced precision in directional changes but reduced swimming speed at lower frequencies. However, at higher frequencies, increased stiffness improved propulsion until excessive stiffness caused buckling, which reduced performance. These findings highlight the importance of balance between stiffness and flexibility in optimizing robotic swimming.

The introduction of a shape-morphing body further expanded the understanding of how morphology influences swimming dynamics. By altering the vertical and lateral profiles of the fish, this study revealed that streamlined shapes such as the flat-flat (FF) configuration reduced drag and increased swimming speed compared to the medium-large (ML) configuration. Central Pat-

tern Generator (CPG) models were effectively utilized to optimize swimming parameters, such as frequency, amplitude, and phase offsets, providing precise control over undulatory motion and achieving the best performance for different body shapes.

Overall, this thesis advances the field of bio-inspired robotics, offering innovative approaches to adaptive design and dynamic locomotion. The research lays the groundwork for future developments in underwater exploration, autonomous systems, and bio-inspired engineering.

## 5.2 Future work

While the findings of this thesis represent progress, they also reveal opportunities for further exploration and refinement. One critical area for improvement is the integration of real-time morphing capabilities. Incorporating on-the-fly actuation of SMMs and TCAs into the robotic fish would enable seamless adaptation to changing environmental conditions and allow for continuous stiffness modulation during swimming. This step would significantly enhance the robot's versatility and operational efficiency.

Refinements to the body morphing design are another avenue for future research. Adding morphing ribs to the fish's head and improving the transitions between body segments could minimize drag and improve the hydrodynamic performance of complex body shapes like the medium-large (ML) configuration. Testing additional shapes inspired by a wider variety of aquatic species could provide further insights into the interplay between morphology and locomotion.

Material advancements also offer promising possibilities. Developing components with greater durability, faster response times, and enhanced flexibility would improve the performance and longevity of morphing mechanisms. Exploring hybrid actuation methods, such as combining SMPs with dielectric elastomers, could enable more complex morphing behaviors and expand the range of achievable deformations.

To realize practical applications, future iterations of the robotic fish should focus on wireless and fully autonomous operation. Achieving a compact, waterproof design with onboard power and

control systems would open pathways for real-world use in environmental monitoring, underwater surveys, and other applications requiring robust, adaptive underwater systems.

Integrating machine learning techniques into the control system could further enhance the robotic fish's capabilities. By using feedback from its environment, the robot could autonomously adjust its stiffness, body shape, and swimming parameters to optimize performance in real-time. This approach would enable greater adaptability and reduce the need for manual programming.

Finally, the embedded morphing scheme demonstrated in this research has applications beyond swimming robotics. Potential uses in fields such as soft robotics, medical devices, aerospace, and automotive engineering warrant further investigation. Extending the principles of adaptive morphing to these domains could lead to innovative solutions for challenges requiring dynamic shape control.

By addressing these areas, future work can build upon the foundations established in this thesis, advancing the state of the art in shape-morphing robotics and its applications.

# Bibliography


[1] R. Baines, S.K. Patiballa, J. Booth, et al. Multi-environment robotic transitions through adaptive morphogenesis. *Nature*, 610:283–289, 2022.

[2] Qiji Ze, Xiao Kuang, Shuai Wu, Pei Wen Janet Wong, Stuart Montgomery, Rundong Zhang, Joshua Kovitz, Fengyuan Yang, H. Qi, and Ruike Zhao. Magnetic shape memory polymers with integrated multifunctional shape manipulation. *Advanced Materials*, 32, 12 2019.

[3] Yong-Jae Kim, Shanbao Cheng, Sangbae Kim, and Karl Iagnemma. A novel layer jamming mechanism with tunable stiffness capability for minimally invasive surgery. *IEEE Transactions on Robotics*, 29:1031–1042, 2013.

[4] Michael McEvoy and Nikolaus Correll. Thermoplastic variable stiffness composites with embedded, networked sensing, actuation, and control. *Journal of Composite Materials*, 49, 06 2014.

[5] Carter Haines, Márcio Lima, Na Li, Geoffrey Spinks, Javad Foroughi, John Madden, Shi Kim, Shaoli Fang, Mônica Andrade, Fatma Göktepe, Ozer Goktepe, Seyed Mirvakili, Sina Naficy, Xavier Lepro, Jiyoung Oh, Mikhail Kozlov, Seon Jeong Kim, Xiuru Xu, Benjamin Swedlove, and Ray Baughman. Artificial muscles from fishing line and sewing thread. *Science (New York, N.Y.)*, 343:868–72, 02 2014.

[6] Yong-Jai Park, Tae Myung Huh, Daegeun Park, and Kyu-Jin Cho. Design of a variable-stiffness flapping mechanism for maximizing the thrust of a bio-inspired underwater robot. *Bioinspiration Biomimetics*, 9(3):036002, mar 2014.

[7] James Tangorra, Patrick Anquetil, Timothy Fofonoff, Angela Chen, Mike Del Zio, and Ian Hunter. The application of conducting polymers to a biorobotic fin propulsor. *Bioinspiration Biomimetics*, 2(2):S6, jun 2007.

[8] Xiaodong Wu and Shugen Ma. Cpg-based control of serpentine locomotion of a snake-like robot. *Mechatronics*, 20(2):326–334, 2010.

[9] Stephen Howe, Kelly Bryant, Andrew Duff, and Henry Astley. Testing the effects of body depth on fish maneuverability via robophysical models. *Bioinspiration Biomimetics*, 17(1):016002, nov 2021.

[10] Di Chen, Bo Wang, Yan Xiong, Jie Zhang, Ru Tong, Yan Meng, and Junzhi Yu. Design and analysis of a novel bionic tensegrity robotic fish with a continuum body. *Biomimetics*, 9(1), 2024.

[11] Zoey S. Davidson, Hamed Shahsavan, Amirreza Aghakhani, Yubing Guo, Lindsey Hines, Yu Xia, Shu Yang, and Metin Sitti. Monolithic shape-programmable dielectric liquid crystal elastomer actuators. *Science Advances*, 5(11):eaay0855, 2019.

[12] J. William Boley, Wim M. van Rees, Charles Lissandrello, Mark N. Horenstein, Ryan L. Truby, Arda Kotikian, Jennifer A. Lewis, and L. Mahadevan. Shape-shifting structured lattices via multimaterial 4d printing. *Proceedings of the National Academy of Sciences*, 116(42):20856–20862, 2019.

[13] J. Sun, B. Tighe, Y. Liu, and J. Zhao. Twisted-and-coiled actuators with free strokes enable soft robots with programmable motions. *Soft Robotics*, 8(2):213–225, 2021.

[14] J. van der Weijde, B. Smit, M. Fritschi, C. van de Kamp, and H. Vallery. Self-sensing of deflection, force, and temperature for joule-heated twisted and coiled polymer muscles via electrical impedance. *IEEE/ASME Transactions on Mechatronics*, 22(3):1268–1275, Jun. 2017.

[15] Xintian Tang, Kai Li, Weishan Chen, Dong Zhou, Shenghui Liu, Jianguo Zhao, and Yingxiang Liu. Temperature self-sensing and closed-loop position control of twisted and coiled actuator. *Sensors and Actuators A: Physical*, 285:319–328, 2019.

[16] Michael C. Yip and Günter Niemeyer. On the control and properties of supercoiled polymer artificial muscles. *IEEE Transactions on Robotics*, 33(3):689–699, 2017.

[17] C. S. Haines and G. Niemeyer. Closed-loop temperature control of nylon artificial muscles. In *2018 IEEE/RSJ International Conference on Intelligent Robots and Systems (IROS)*. IEEE, Oct. 2018.

[18] Lianjun Wu and Yonas Tadesse. Modeling of the electrical resistance of tcp muscle. In *ASME 2017 International Mechanical Engineering Congress and Exposition*, page V04AT05A024, 11 2017.

[19] Jiefeng Sun and Jianguo Zhao. Integrated actuation and self-sensing for twisted-and-coiled actuators with applications to innervated soft robots. In *2020 IEEE/RSJ International Conference on Intelligent Robots and Systems (IROS)*, pages 8795–8800, 2020.

[20] Sanaz Bazaz Behbahani and Xiaobo Tan. Design and dynamic modeling of electrorheological fluid-based variable-stiffness fin for robotic fish. *Smart Materials and Structures*, 26(8):085014, jul 2017.

[21] Hongxiu Zhu, Yupeng Sha, and Haonan Ding. Research on fish variable stiffness: A review. In *2021 IEEE International Conference on Unmanned Systems (ICUS)*, pages 224–231, 2021.

[22] Daniel Quinn and George Lauder. Tunable stiffness in fish robotics: mechanisms and advantages. *Bioinspiration  Biomimetics*, 17(1):011002, dec 2021.

[23] Qianqian Zou, Chao Zhou, Ben Lu, Xiaocun Liao, and Zhuoliang Zhang. Tail-stiffness optimization for a flexible robotic fish. *Bioinspiration  Biomimetics*, 17(6):066003, sep 2022.

[24] Sunil Kumar Rajendran and Feitian Zhang. Developing a novel robotic fish with antagonistic artificial muscle actuators. page V001T30A011, 10 2017.

[25] Kara L Feilich and George V Lauder. Passive mechanical models of fish caudal fins: effects of shape and stiffness on self-propulsion. *Bioinspiration Biomimetics*, 10(3):036002, apr 2015.

[26] Mohamad Omari, Mehdi Ghommem, Lotfi Romdhane, and Muhammad R. Hajj. Performance analysis of bio-inspired transformable robotic fish tail. *Ocean Engineering*, 244:110406, 2022.

[27] Kiyotoshi Matsuoka. Sustained oscillations generated by mutually inhibiting neurons with adaptation. *Biological Cybernetics*, 52(6):367–376, October 1985.

[28] Paul W. Webb. Form and function in fish swimming. *Scientific American*, 251(1):72–83, 1984.

[29] P. R. Bandyopadhyay, J. M. Castano, J. Q. Rice, R. B. Philips, W. H. Nedderman, and W. K. Macy. Low-Speed Maneuvering Hydrodynamics of Fish and Small Underwater Vehicles. *Journal of Fluids Engineering*, 119(1):136–144, 03 1997.

[30] Paul W. Webb. Stability and maneuverability. In *Fish Biomechanics*, volume 23 of *Fish Physiology*, pages 281–332. Academic Press, 2005.

[31] Lu Cai, Jihua Chen, David Johnson, Zhiying Tu, and Yingping Huang. Effect of body length on swimming capability and vertical slot fishway design. *Global Ecology and Conservation*, 22:e00990, 2020.

[32] Vladislav Kopman and Maurizio Porfiri. Design, modeling, and characterization of a miniature robotic fish for research and education in biomimetics and bioinspiration. *IEEE/ASME Transactions on Mechatronics*, 18(2):471–483, 2013.

[33] Sijia Liu, Yingjie Wang, Zhennan Li, Miao Jin, Lei Ren, and Chunbao Liu. A fluid-driven soft robotic fish inspired by fish muscle architecture. *Bioinspiration Biomimetics*, 17(2):026009, feb 2022.

[34] William Coral, Claudio Rossi, Oscar M Curet, and Diego Castro. Design and assessment of a flexible fish robot actuated by shape memory alloys. *Bioinspiration Biomimetics*, 13(5):056009, jul 2018.

[35] Tsam Lung You, Jonathan Rossiter, and Hemma Philamore. Robotic fish driven by twisted and coiled polymer actuators at high frequencies. In *2023 IEEE International Conference on Soft Robotics (RoboSoft)*, pages 1–6, 2023.

[36] JR. LONG, JOHN H. and KAREN S. NIPPER. The importance of body stiffness in undulatory propulsion1. *American Zoologist*, 36(6):678–694, 08 2015.

[37] Li Kangkang, Hongzhou Jiang, Siyu Wang, and Jianmin Yu. A soft robotic fish with variable-stiffness decoupled mechanisms. *Journal of Bionic Engineering*, 15:599–609, 07 2018.

[38] Bingxing Chen and Hongzhou Jiang. Body stiffness variation of a tensegrity robotic fish using antagonistic stiffness in a kinematically singular configuration. *IEEE Transactions on Robotics*, 37(5):1712–1727, 2021.

[39] Alfonso Parra Rubio, Dixia Fan, Benjamin Jenett, José del Águila Ferrandis, Filippos Tourlomousis, Amira Abdel-Rahman, David Preiss, Jiri Zemánek, Michael Triantafyllou, and Neil Gershenfeld. Modular morphing lattices for large-scale underwater continuum robotic structures. *Soft Robotics*, 10(4):724–736, 2023. PMID: 36730716.

[40] Hongbing Huang, Zhonglu Lin, Wei Zheng, Jinhu Zhang, Wei Zhou, and Yu Zhang. How biomimetic morphing dorsal fin affects the swimming performance of a free-swimming tuna robot, 2023.

[41] Valerio Pini, JJ Ruz, Priscila M Kosaka, O Malvar, Montserrat Calleja, and J Tamayo. How two-dimensional bending can extraordinarily stiffen thin sheets. *Scientific reports*, 6(1):29627, 2016.